UNIVERSITÀ DEGLI STUDI DI MILANO

Scuola di Dottorato in Scienze Farmacologiche

Dipartimento di Biotecnologie Mediche e Medicina Traslazionale

CORSO DI DOTTORATO IN SCIENZE FARMACOLOGICHE

Ciclo XXVIII

A NANOTECHNOLOGY APPROACH FOR GLIOBLASTOMA TARGETED THERAPY

BIO/14

MATTEO TAMBORINI

MATRICOLA: R10181

Director of Studies: **Prof. Alberto CORSINI**

Tutor: **Prof. Alberto PANERAI**

Co-tutor: **Dtt.ssa Cecilia GOTTI**

A.A. 2014 / 2015

Table of contents

Abstract

Glioblastoma multiforme (GBM) is an extremely aggressive type of glioma. Life expectancy is around two years after diagnosis, due to recidivism and to the presence of the blood brain barrier (BBB) restricting the amount of drugs which arrive at the residual cancer cells, thus contributing to chemotherapies failure. To overcome the impediment imposed by the BBB, we have investigated the use of nanotechnologies in synergy with radiotherapy as a prospective strategy for GBM treatment. We have used poly(lactic-co-glycolic acid) (PLGA) nanoparticles (PNP) conjugated to the peptide chlorotoxin (CTX), which has been shown to recognize and selectively bind to glioma cells. Silver nanoparticles have been encapsulated inside the functionalized nanoparticles (Ag-PNP-CTX), to allow detection of cellular uptake and quantification by means of confocal microscopy, both in vitro and in vivo. In vitro experiments, involving 3 different human glioblastoma cell lines, have shown that the cytoplasmic uptake of Ag-PNP-CTX is higher than that of non-functionalized nanoparticles. Experiments performed in vivo have shown high efficiency of Ag-NP-CTX particles in targeting tumor cells; however, they have been shown to be scarcely able to cross the blood brain barrier at the healthy brain level, where scattered metastatic cells are present too. A single x-rays administration on the whole brain, carried out twenty hours before the injection of the nanoparticles, has been shown to increase the levels of expression of the CTX targets MMP-2 e ClC-3. Moreover, through an alteration of BBB permeability, it has been shown to potentially increase the quantity of internalized Ag-PNP-CTX also in dispersed cells, and to lead to significant results in inhibiting tumor growth in vivo. Notably, the administration of Ag-PNP-CTX to irradiated tumor cells decreases the MMP-2 extracellular activity. By targeting scattered GBM cells and limiting MMP-2 activity, the synergic use of nanovectors conjugated with CTX and radiotherapy may represent an efficient therapeutic approach to GBM treatment.

1 Introduction

1.1 Brain tumors

Cases of primary malignant central nervous system (CNS) tumors constitute about 2% of all cases of cancer [1].

Intracranial tumors can arise in adulthood and children or adolescents. They are the primary cause of death in children and the third primary cause of death for adolescents and adults [2, 3].

Primary CNS tumors comprise a wide range of pathological entities, each with a distinct natural history. CNS tumors can be classified as gliomas or non-gliomas [4]. Non-gliomas can originate from different brain tissues. For example meningiomas, a benign form of cancer, originate in the dura [5], while medulloblastoma [6], and cerebral neuroblastoma are classified as primitive neuroectodermal tumors [7].

Tumors originating from glial cells are called gliomas and represent about 80% of all malignant CNS tumors [8]. The most common gliomas are astrocytomas, including glioblastoma multiforme (GBM), oligodendrogliomas, and ependymomas [8-9].

A brain tumors classification drafted in 2007 by World Health Organization (WHO), also supplies objective criteria to categorize histologic grade of head cancer:

- Low grade I tumors are characterized by lesions with low proliferative potential (i.e. pilocytic astrocytomas).
- Low grade II is a type of cancer with low proliferative potential with infiltration tendencies and cytologic anomaly (i.e. astrocytoma).
- High grade III tumors are characterized by lesions with anaplastic evidence and mitotic activity (i.e. anaplastic astrocytoma).
- High grade IV tumors are characterized by lesions with nuclear anomaly, cellular pleomorphism, mitotic activity, microvascular proliferation and/or necrosis (i.e. GBM) [10-11].

Astrocytic tumors can be distinguished into two distinct categories based on how they interact with their immediate microenvironment, namely diffuse and localized astrocytomas. Localized astrocytomas have a circumscribed pattern of growth and limited invasive potential, whereas diffuse astrocytomas are characterized by their cellular infiltration of the peritumoral margin and disperse to distant sites, regardless of tumor grade [12-13]. Although astrocytic tumors of all three higher grades are invasive, the higher-grade tumors (i.e., grades III and IV) are progressively more proliferative and result in a shorter time to tumor recurrence than lower-grade tumors [8]. All glial tumors (except for [WHO grade I]) recur at high frequency after treatment with surgery, radiation, and chemotherapy and are essentially incurable [14].

1.2 Glioblastoma Multiforme

1.2.1 Introduction

Glioblastoma multiforme (GBM) is the most common primary brain neoplasia which is mostly found in 55-years adults, but which can arise in younger (children and adolescents) population too. It is among the deadliest of all human cancers with an overall 5-year survival rate of less than 3,3% [15]. It represents 12-15% of all intracranial neoplasia and 60-75% of the astrocytic tumors [16]. GBM can be a primary tumor, if it arises without previous evidence of disease, otherwise it can develop from lower grade gliomas (secondary GBM) [17].

GBM is characterized by remarkable biological heterogeneity and poor response to currently available treatments [18]. Even if the tumor responds well to initial treatments and is seemingly disappeared on follow-up scanning, recurrence is inevitable locally, often within 2 cm of the original tumor, or at distant sites within the brain [20]. The median survival time of GBM patients with the best currently available therapy is approximately 14,6 months [15].

The causes of treatment failure, disease progression, and recurrence flow from the biological features of GBM. Critical GBM peculiarity is the high level of proliferation, invasiveness, angiogenesis, stemness [19].

1.2.2 Invasion and metastatic potential

GBM is a highly proliferative and invasive type of cancer [18]. Even though it rarely metastasizes out of the CNS, GBM cells have an excellent infiltrating ability at the brain level [21]. Changes of shape, volume, morphology and the formation of membrane protrusions allow cancer cells to invade brain parenchyma, through the perivascular space or through the extracellular matrix (ECM) [22]. These actin rich protrusions, termed invadopodia in cancer cells [23], constitute a key step in invasion processes: they help cells move forward and permit them to attach to the ECM and degrade it [24]. The invadopodia ability to digest ECM is attributed to the presence of ECM degrading enzymes such as matrix-metalloproteinases (MMPs). Furthermore, MMPs can be released from protrusions to facilitate invasion [25]. Indeed, there is evidence of involvement of MMPs in ECM degradation and of overexpression of several MMPs in cancer cells, including glioma cells [26]. Glioma cells movements is determined by ECM deterioration, and promoted by the presence of the chloride channels that actively contribute to changes in cell shape and volume [27].

1.2.3 MMP2

MMPs constitute a family of proteinases which includes 22 enzymes [28-29-30-31]. MMPs named according to the order of their discovery and can be distinguished into different subclasses on the basis of their substrate specificity (collagenases, gelatinases, matrylisn, metalloelastase, enamelysin) [32]. In the CNS, over 10 different types of MMPs have been found [33] and their role in CNS pathology has been demonstrated [34] In particular, MMP2 (72 KDa gelatinase type A) is involved in cancer progression, invasion, metastasis, angiogenesis, and survival [35, 36, 37].

MMP2 is a Zn^{+2} dependent endopeptidase and, similarly to all MMPs, is synthesized and secreted as zymogen form and its regulation occurs at different levels [38]. Whole activation is allowed by activating factors that cause pro-peptide domain removal (see Figure 1 for more detailed mechanisms explanation) [38-39].

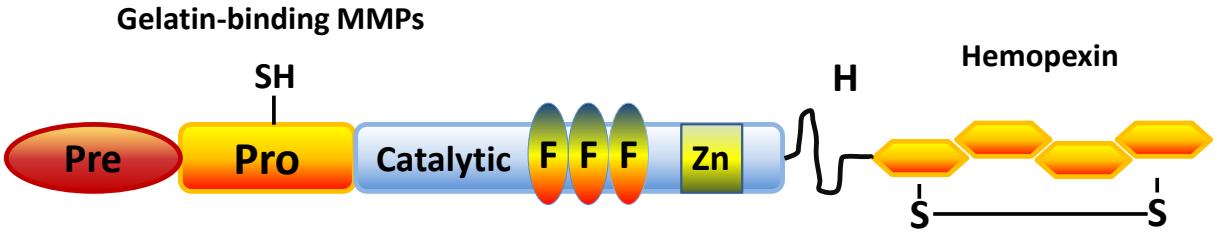

Figure 1. Schematic representation of MMP2 domains. Pre-domain N-terminal signal sequence that directs the protein to the endoplasmic reticulum. Pro-domain that contains a highly conserved sequence with unpaired cysteine sulfhydryl groups that interact with the active site zinc maintaining the MMP2 in latent form (the cysteine switch). Catalytic domain contains the conserved zinc-binding region, three gelatin-binding fibronectin types II repeats and also have a series of three head-to-tail cysteine-rich repeats within its catalytic domain. These inserts resemble the collagen-binding type II repeats of fibronectin and are indispensable to bind and cleave collagen. Hemopexin domain is folded into a four-bladed propeller structure. The hemopexin domain is required for TIMP2 (Tissue Inhibitors of Metalloproteinases2) binding (via the C-terminal), the binding of substrates, membrane activation, and some proteolytic activities. Figure adapted from Sternlicht et al., 2001 [39].

The regulation of MM2 is higly regulate, in GBM context can occur an over expression of MMP2 and its activity [40-41]. MMP2 is regulated at different levels:

1. transcription level
2. post-translational level
3. interaction with tissues inhibitors

1. MMP2 transcription level can be modulated by many substances such as fibronectin in many types of cancer cells including gliomas [42-43-44-45] by complex signals induced by ECM proteins like osteopontin, various cytokines including IL-8 that is overexpressed in glioma cell [46] by epigenetic mechanisms [47-48], and also by growth factors such as EGF [49].

2. MMP2 activity regulation can occur at post-translational level due to different proteases [50] and by phosphorylation status [51]. MMP2 contains 29 potential phosphorylation sites a has been shown that the phosphorylation status of MMP2 significantly affects its enzymatic properties improving his activity [51-52].

3. MMP2 activity is regulated by its interaction with tissue inhibitors of metalloproteinases (TIMPS) [53-54]. TIMP2 is specific inhibitor of MMP2 (see figure 2) [55]. However, TIMP2 have a double role in MMP2: inhibition and activation [56].

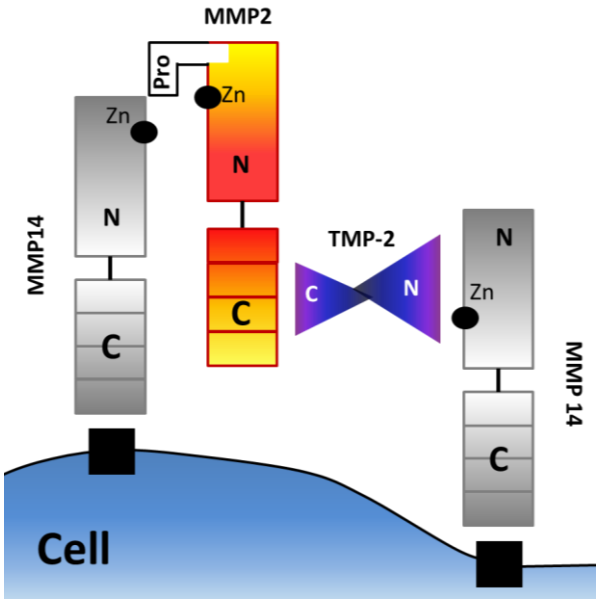

Figure 2. MMP14 - TIMP2 – MMP2 ternary complex schematic representation. TIMP2 bind through its N-terminal three loops to the MMP14 catalytic domain. Figure adapted from Murphy et al., 1997 [56].

In the case of TIMP2 as MMP2 inhibitor, in very general terms, it is possible to explain MMP2 regulation on the basis of TIMP2 expression levels as follows.

- High TIMP2 levels: MMP2 is inhibited. At the membrane level, TIMP2, pro-MMP2 and type 1-matrix metalloproteinase (MMP14) form a ternary complex [57] (Fig. 2); two MMP14 molecules inhibit MMP2 activation with the result in pro-MMP2 recruitment and accumulation [57].

- Low levels of TIMP2: MMP2 is activated. There is not a MMP14-MMP2 ternary complex and MMP14 can mediate MMP-2 activation. A free MMP14 molecule cleaves partially MMP2 the pro-peptide region [56]. Complete pro-peptide removal is due to the action of the MMP2 intermediate or to other active MMPs ("stepwise activation" mechanism) [58].

In normal tissues which express low levels of MMP2 and MMP14, even low amounts of TIMP2 are sufficient to inhibit MMP2 activation [57]. However in GBM cells, where

MMP2 and MMP14 are upregulated [57], the amount of TIMP2 is the main responsible for balancing MMP2 activation level [59].
GBM cells, such as U87MG cell line that overexpress MMP2 and MMP14 but secrete TIMP2 at low levels, are able to induce low MMP2 activation [57].
In cases of higher upregulation of TIMP2 level expression, MMP14 /TIMP2/proMMP2 complexes are more often found at the membrane level resulting in an increased presence of MMP2 active form [57].

MMP2 is upregulated in high-grade gliomas, such as GBM, whereas its level of expression is lower in lower-grade types [41].
A correlation between MMP2 level of expression and the ability of different glioma cells to migrate across a synthetic basement membrane in vitro has been established [40].
MMP2 invasive properties arise from its ability to digest a large number of ECM components including type I, II, III; IV, V and XI collagens, laminin and aggrecan core protein [60].

1.2.4 CLC-3

The family of chloride channels (ClCs) is a highly conserved cluster of voltage-gated channels and has 9 members [61]. ClCs are involved in the regulation of cell volume, control of electrical excitability, trans-epithelial transport [63], and cell cycle progression [64]. The role of ClCs in bypassing cell cycle checkpoint can explain their implication on the oncogenesis process [65-56].
The CIC-3 chloride channel, in particular, is normally expressed in the SNC in the synaptic vesicles [67-68], in the membranes of the late endosomes [69-70] and also in glial cells [71]. Being up-regulated in glioma membranes [72-73], it has been supposed to be actively involved in the glioma cells invasive process [74] and to play an important role in facilitating migrating behavior of GBM cells [27].

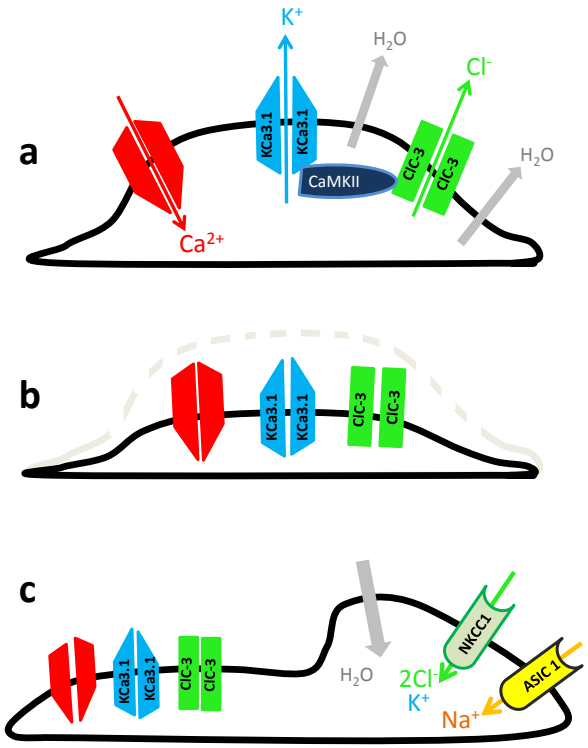

Figure 3 - Schematic representation of ClC-3 mediated glioma cells motility processes. a) Stimulation of G protein-coupled receptors (GPCRs) causes an increase of intracellular Ca2+ concentration in glioma cells, leading to Ca2+-dependent activation of Ca2+/calmodulin-dependent protein kinase II (CaMKII)-dependent ClC3 and KCa3.1 channel opening. This leads to the efflux of Cl− and K+, obligating water to flow down its osmotic gradient and leave the cell. b) The consequent decrease in cytoplasmic volume enables it to squeeze into adjacent spaces and to pass barriers. c) The successive ion influx mediated by the Na+–K+–Cl− cotransporter 1 (NKCC1) and the acid-sensing ion channel 1 (ASIC1) causes water influx and, consequently, cytoplasmic volume increase. Figure adapted from Cuddapah et al., 2010 [75].

ClC-3 channels are crucially involved in the motility of glioma cells. As shown in Figure 3, cell movements are caused by water efflux due, among other factors, to the opening of the overexpressed ClC-3 channels. These events cause a decrease of cytoplasmic volume, making the cell able to squeeze into small spaces. The successive volume increase, due to influx of Na^+, K^+ and $2Cl^-$ causing, in turn, water influx, enables the cell to move forward and pass barriers (Figure 3) [72,75].

ClC-3 can facilitate invasiveness also by forming complexes with MMP2, TIMP2, MMP14, αvβ3 integrin, BK potassium channel and aquaporin-4 (AQP-4) in lipid rafts of invadipodia [76].

1.3 Therapy of Glioblastoma Multiforme

1.3.1 Introduction

Standard GBM treatment consists of surgical resection followed by 6 weeks of radiotherapy with concomitant Temozolomide (TMZ) and by adjuvant TMZ as single agent [77].

Even when treated aggressively, GMB recurs and this is the cause of the poor prognosis. The area of recurrence develops at the borders of the surgical cavity, over 90% of the cases within 2 cm of the original tumor, or at distant sites within the brain at later stage [20].

In case of recurrence, a limited number of treatments are available.

Factors that can influence the therapeutical response are the following: patient age, tumor location, the Karnofsky Performance Status, lesion radiologic characteristics, amplitude of surgical resection, proliferation index, the metilation status of the promoter of gene for the metil-guanin-metil-transferasi (MGMT) and the status of IDH1/2 [78,79].

1.3.2 Surgery

Surgery is the early therapy step for all patients with primary brain cancer. Surgery can be curative for many benign tumors, such as meningiomas [80] but not so efficient as far as high grade gliomas are concerned. This failure is due by infiltrative nature of high grade gliomas that makes complete surgical removal impossible [81]. Surgical removal currently is the most effective treatment: survival time is correlated with the amount of resected tumor mass [82].

In high grade gliomas cases, the goal of surgery is limited to eliminating neurologic symptoms due by cancer mass, to obtaining histologic diagnosis from the biopsy, to promoting reduction of cancer cells, and to treating hydrocephalus if present [82].

1.3.3 Radiotherapy

Ionizing radiations are currently employed on the part of the brain which has been subjected to surgical resection [15].

The main role of radiotherapy (RT) is to damage DNA of infiltrating cells which cannot be eradicated by the surgery, as well as of cells spreading from distant sites of surgery [83]. RT is also effective in blood-brain barrier (BBB) disruption in dose time dependent [84]. This phenomenon can lead to a more effective chemotherapic drugs (especially of hydrophilic compounds) delivery [85].
Different approaches have been recently developed in order to improve therapy effectiveness, including:

- **Fractionated radiotherapy**. It consists in fractionating the total amount of therapeutical radiation into several doses. For example, a total dose of 60 Gy fractionated into 2 Gy doses for 30 days after surgery [20,77] are administred on the part subjected to surgery and on the immediate surroundings (2 cm over the surgical border) [86].
- **Ultrafractionated radiation therapy.** It is a system consisting of radiotherapy low doses (<0.75 Gy) administered several times daily (3 daily doses every 4 hours for 5 days per week). The treatment lasts 6–7 weeks (90 fractions for a total of 67.5 Gy) [86].
- **Stereotactic radiosurgery (SRS).** SRS is a form of radiation therapy that consists in high-power energy administration (24 Gy, 18 Gy, or 15 Gy) focused on a small area (diameter between 20-40 mm in diameter) [87]. SRS is usually used for the treatment of one to few brain metastases in a single session or when tumor cannot be removed [88].
- **Stereotactic radiotherapy.** Stereotactic radiotherapy is a treatment used for small tumors which are impossible to eradicate by surgery. By means of a linear accelerator (LINAC), low doses of ionizing radiations are delivered from different angles converging in a specific small area (diameter between 20- 40 mm in diameter) [87]. The result is a high amount of radiations delivered in a precise area minimizing damage to healthy surrounding tissues. Generally, the treatment is fractionated into 3 and 30 daily doses [89].

The effectiveness of RT for high grade gliomas has been confirmed by many experimental studies [15, 90-94]. For example, in survival times after surgery and radiotherapy, radiotherapy only, surgery only, and no therapy have been assessed

through univariate, multivariate, and Kaplan–Meier analyses: the results have been 7 months, 4 months, 2 months, and 1 month, respectively. Nevertheless, there are also adverse effects [90]. One of the most significant ones is the tendency to induce overexpression of MMP2 [95] and MMP9, as well as to increase the expression of TIMP2 [96, 97] all molecules involved in invasivity processes. In principle, therefore, radiations can increase the probability of recidivism [98].

1.3.4 Chemotherapeutics

TMZ, administered with RT, is the most effective drug for GBM treatment. As there is no equally effective alternative therapy in case of drug resistance [95], the many clinical trials are under investigation. Some of them consist in subjecting t he patient to a variety of dosing schedules in which the duration of exposure and the cumulative dose of TMZ is increased, with the purpose of improving antitumor activity and overcoming resistance [99]. Other clinical trials involve targeted therapies in combination with cytotoxic chemotherapy and radiotherapy in order to bypass tumor resistance [100]. These include Epidermal Growth Factor Receptor Inhibitors, Platelet-derived Growth Factor Inhibitors, Vascular Endothelial Growth Factor/ Vascular Endothelial Growth Factor Receptor Inhibitors, Mammalian Target of Rapamycin Inhibitors, Protein Kinase C, RAF-MEK-ERK, and Integrin Inhibitors. Most of the targeted therapy validate on phase II clinical trials have not given benefits in survival ratio. Better drugs strategies are represented by the combination of multitargeted drugs with cytotoxic chemotherapy and radiotherapy [for a review on targeted therapies for GBM see100].

1.3.5 Resistance to radiotherapy and chemotherapy

Recidivism is due to the fact that not all malignant cells are totally removed by the currently available pharmacological treatments.
The reasons of drug failure can be grouped as follows:

1) intrinsic biology of GBM cells;
2) GBM micro-environment;

3) Chemoresistence induced by pharmacological treatment.

As far as the first point is concerned, GBM cells show mutations which ultimately decrease the effectiveness of the current therapies. The overexpression of factor tyrosine kinase receptor (TKR) pathways and the upregulation of several growth factors such as EGF contribute to lead resistance to drugs [101].

In addition the presence of the ATP-binding cassette (ABC) transporter family (P-glycoprotein, P-gp), and of the multi-drug resistance protein (MRP) [102], reduce the drugs efficacy pushing drugs out of the cell [103]. Moreover, the presence of integrins β1 [104], αvβ3, and αvβ5 [105] contrast the cytotoxic effects of the drugs by facilitating cell proliferation and preventing apoptosis [106]. Other element responsible for drug failure is the presence of glioblastoma staminal cells (GSCs) [107]. GSCs resistance to therapy is higher than that of more differentiated GBM cells, both in vivo and in vitro [108]. This is due, for example, to the upregulation in GSCs of anti-apoptotic proteins (miR-21 and Bcl-2 for example) [108] and by upregulation of DNA repair ability [109,110].

Drug failure can be caused by microenvironmental factors too [111]. Some areas in the microenvironment are hypoxic. GBM cells in hypoxic areas show low amount of proliferation and have a slower metabolism; therefore, they are non-responsive to the anti-cancer drugs which are effective on highly proliferating cells [112]. Moreover, they show an increase of pro-survival responses induced by transcription of several genes, which include the family of hypoxia inducible factors (HIFs) [113].

A third sort of factors responsible for drug failure concern the specific target of the drug and the effects of the drug in promoting resistance. These factors can be intrinsic or acquired [113]. Intrinsic factors are related to mutations of the specific molecules. For example, overexpression of the DNA repair protein O6-methylguanine methyltransferase (MGMT) makes TMZ ineffective, similarly to every other alchilating agents [114]. Acquired resistance occurs when initially responsive cells progressively become non-responsive [114-115].

Drug resistance can be also caused by radiotherapy (ref): ionizing radiations can induce survival of cancer cells by increasing the level of expression of several growth factors and proteins such as the epidermal growth factor receptor (EGFR) [116] and

vascular endothelial growth factor (VEGF) [117], which are known to have anti-apoptotic effects [101].

1.4 The blood brain barrier

1.4.1 Introduction

One of the major limitations of chemotherapy in brain tumors is represented by the inefficient passage of drugs across the blood brain barrier (BBB). For this reason, drugs cannot reach niches of GBM cells infiltrated in the healthy parenchima and protected by the BBB [118-120]. Moreover, BBB cells tend to extrude drugs due to the action of P-glycoproteins (Pgp/ABCB1), which are multidrug resistance-related proteins [121]

BBB is an active, dynamic anatomical-functional unit which regulates exchanges between blood vessels and the brain parenchima [120]. It plays a key role in brain homeostasis and provides protection against many toxic compounds and pathogens [121]. In addition, the BBB regulates and supply nutrients to the brain by specific transport systems [122].

BBB is made by cellular and non-cellular components [123]. The cellular components include neurons, microglia, pericytes, astrocytes and endothelial cells (ECs) (Figure 4) [124].

ECs compose the SNC endothelium and constitute key structural components of the BBB [125]. ECs have an uniform thickness, low pinocytotic activity [126,127] and there is no fenestration between adjacent cells, thus leading to a considerable reduction of the paracellular diffusion of hydrophilic solutes [128]. Due to these features, ECs are able to strictly regulate the selective transport of substances from blood to brain and from the parenchyma to blood [129].

Astrocytes play a fundamental role in the functionality of BBB. Their endfeet are apposed to the BBB endothelium and to the basement membrane, thus crucially contributing to maintaining its integrity [128].

Astrocytes also crucially contribute to proteoglycan synthesis and to the subsequent increase in brain microvascular endothelial cells (BMVEC) charge selectivity; they also play an important role in every BBB function and modulation [129].

The non-cellular component is composed by agrin, heparan sulphate proteoglycan, an extracellular matrix compound [130], and by the basement membrane which is an essential BBB component surrounding BMVEC and securing the BBB cells in place [131]. BMVEC, pericytes and astrocytes all generate and maintain the basement membrane. The basement mebrane is constituted by fibronectin, laminin l a noncollagenous glycoprotein [132,133] collagen, and elastin [134].

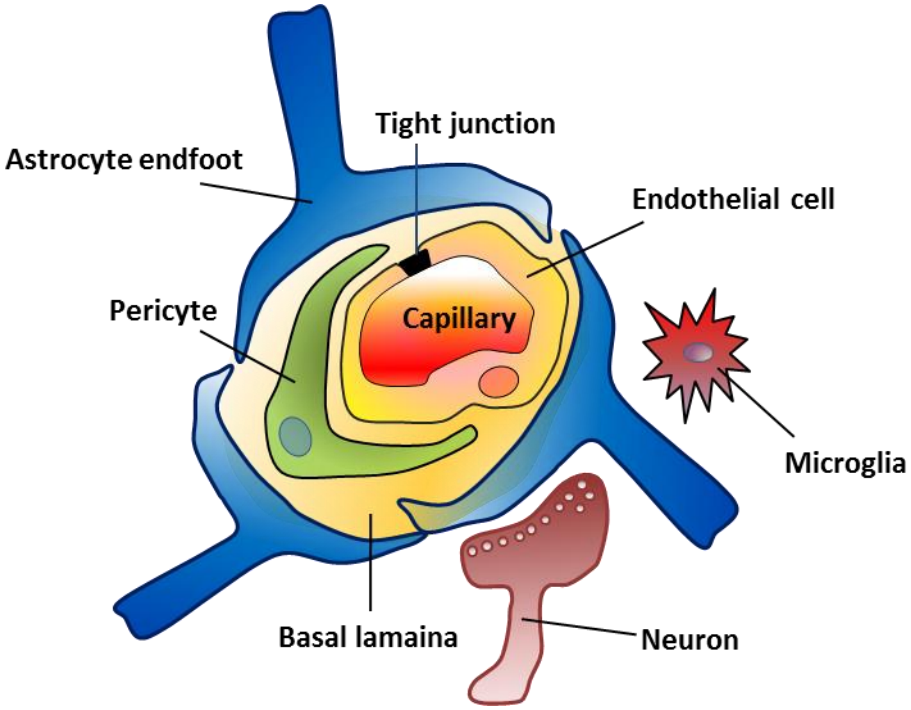

Figure 4. Schematic structure of the main BBB components. Neurons regulate the function of blood vessels by triggering expression of EC enzymes. Microglia contributes to BBB properties by interacting with EC. Pericytes are physically associated with the endothelium and synthesizes most elements of the basement membranes, such as some kinds of proteoglycans and laminal proteins. Figure adapted from Abbott et al., 2010 [135].

Brain microvascular characteristics result from interactions of these cells with the basement membrane [135,136]. All these cells and basement membranes constitute the neurovascular unit (NVU) which is essential for physiological CNS function [123].

1.4.2 Tight junctions

Critical components of The BBB are represented by tight junctions (TJs or “zonulae occludentes”) present between adjacent endothelial cells. They play a pivotal role in BBB selective permeability by reducing paracellular diffusion of polar solutes and macromolecules [137].

Tight junctions consist of a protein complex including occludin, claudins 3, caludins 5 and junctional adhesion molecules (JAMs) [136]. Claudins 3 and 5, which constitute the most effective factor in limiting paracellular diffusion, associate and bind to one another across the intercellular scaffolding and regulatory proteins ZO-1, ZO-2, ZO-3 and cingulin (Figure 5) [134].

Some properties of the BBB tight junctions are highly sensitive to stimuli coming from the microenvironment, and can be modulated “*minute-to-minute*” resulting in functional changes of paracellular pathways [138]. Claudins and occludins configurations change modifying the tight junctional properties.

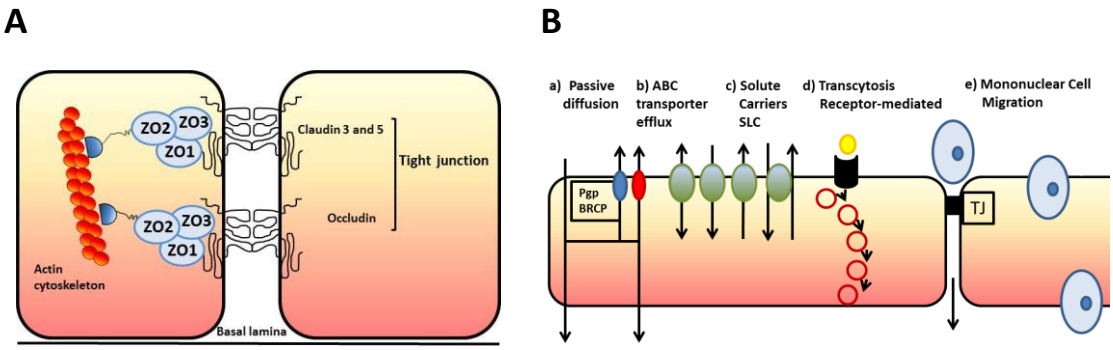

Figure 5. Schematic structure of BBB tight junctions. A) Tight junctions comprise occludin, claudins 3 and claudin 5. Claudins and occludins link the scaffolding proteins ZO-1, ZO-2 and ZO-3, connected by means of cingulin dimers to actin/myosin. B) Transport across the BBB. (a) Passive diffusion of lipophilic solutes. (b) Active efflux carriers ABC transporters, such as Pgp and BCRP, can stop solutes and pump them out of the cell. (c) Carrier mediated influx via solute carriers (SLCs) can be passive or active and can transport many essential polar molecules such as glucose, amino acids and nucleosides into the CNS. (d) transcitosys receptor mediated (RMT) mediates transport of various macromolecules, including peptides and proteins, across the endothelium (transcytosis). (e) Leukocytes cross the BBB either by a process of diapedesis through the endothelial cells, via CD99 receptor, or through modified tight junctions. Figure adapted from Begley et al., 2003 [138].

1.4.3 Blood–brain barrier in glioblastoma multiforme

An important feature of GBM is its high grade of vascularization, due to its tendency to carry out angiogenetic processes [139]. Unlike normal cerebral vessels, GBM neo vessels are characterized by morphological and functional alterations [140].

The most common characteristics of GBM blood vessel are [140]:

- formation of fenestrations;
- alterations of the tight junctions;
- number of caveolae and mitochondria;
- thickness of the subendothelial basal lamina;
- increase of the perivascular space.

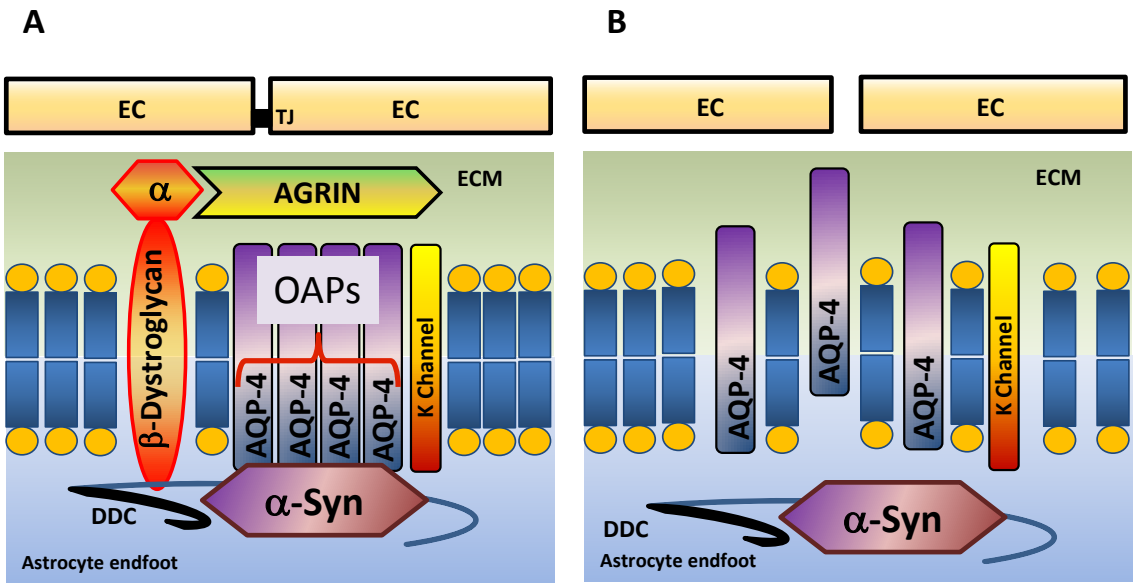

Figure 6. Schematic view of the relation between glial endfoot and ECs. A) Astrocytes endfoot in healty BBB. Astrocytes endfeet are closely associated with endothelial cells (ECs) .β-dystroglycan is a membrane protein in contact with α-dystroglycan (outside) and the dystrophin–dystroglycan complex (DDC; inside). α-syntrophin binds to AQP4. AQP4 can arrange in complexes named orthogonal arrays of particles (OAPs). Agrin binds with α-dystroglycan,. However, it is connected to AQP4 by an α-dystroglycan to α-syntrophin bridge. K+ channels in the endfeet co-localize with aquaporin 4 (AQP4) (K+ and AQP4 have similar conductivity distribution. K+ ions, whose extracellular concentration is increased by neuronal activity, are taken up by astrocytes; K+ uptake is accompanied by water efflux through AQP4. The correct positioning of K+ channels and AQP4 is due to the presence of agrin, an heparan sulphate proteoglycan, extracellular matrix compound and laminin noncollagenous glycoprotein . B) Astrocytes endfoot in glioblastoma BBB. MMP3 cleaves agrin and MMP2/9 cleave dystroglycan. MMPs digestion leads to a loss of OAPs and to a

loss of AQP4-polarity due to the loss of DDC scaffolding quality. Figure adapted from Wolburg et al., 2012 [140].

BBB vessels can be destroyed by the presence of GBM cells. MMPs, upregulated in GBM cells, are involved in BBB disruption [141-142]. Similarly to MMP9 and MMP2, MMP-3 are upregulated in GBM [141]. MMP3 cleaves agrin and MMP2 and MMP9 destroy dystroglycan at the level of astrocytic endfoot (Figure 6) leanding an alteration of potassium and water channel [140]. The result is the detachment of astrocytic endfeet from the vessel and from the basal lamina, the disruption of TJs of ECs cells and the breakdown of the BBB by runaway influx of extracellular water into the brain parenchyma (vasogenic edema) [140,141].
The MMPs activity damages the ECM too resulting in increase of thickness and agrin downregulation [142]. The basement membrane digestion contributes to TJs deregulation [143,144]. Accordingly, extracellular matrix disruption is strongly associated with BBB permeability increase not only in GBM but also in several pathological situations [144].

1.4.4 Effects of ionizing radiation on the BBB

Ionizing radiation can impair the integrity of the BBB [145]. It has been shown that in a murine model, a single dose of 0,1 Gy, 2 Gy or 10 Gy is able to increase the BBB permeability determining an extravasation of Albumin. The time window of BBB opening depends on age, on dose and on administered dose number of radiations [145, 146].
Radiations cause permeability of BBB modulation, leading changes in morphological structures of ECs cells and surrounding vessel astrocytes, and leading senescence in ECs cells [146]. The increased permeability of BBB caused by radiations is associate with disruption of TJs between adjacent ECs in vitro [146].

1.5 Polymeric nanocarriers

1.5.1 Introduction

Given the complexity for most drugs to reach the brain and bypass the BBB, the use of nanotechnological approaches, and in particular nanoparticles, has been proposed as promising and alternative therapeutic strategy [147].

Nanotechnology has been suggested for selectively deliver contrast imaging and anti-cancer agents into tumor cells with the advantage of not affecting normal healthy tissues and cells [148].

Nanoparticles can vary in chemical composition in size and shape and their surface may be modified [149]. Different compositions confer to nanoparticles specific abilities; for example the peptides addition on the nanoparticles external surface can address them to a specific target [149]. Nanoparticles can be achieved to permeate the brain bypassing through endothelial cells by transcytosis, opening the tight junctions of brain capillaries or adhering to the vessels walls and crossing the BBB by virtue of osmosis [149, 150].

Nanoparticles can act as a tumor-specific drug delivery vehicle working as carriers. Drugs can be encapsulated within the nanocarrier which can be shaped as a cage, a shell, a bubble, or as other kinds of forms [151].

Nanocarrier-based drug delivery into the tumor occurs through passive and active targeting [152]. Passive targeting is mediated by the inherent features of the tumor itself to retain drug-carrying nanoparticles and it is due to the increased permeability and retention (EPR) effect due by fenestrated angiogenic vessels [153]. Tumor blood vessels, contrary to normal, have 600 to 800 nm wide gaps between adjacent endothelial cells, leading to a faulty vascular system enabling nanoparticles to extravasate into the extravascular area and gather into tumor tissues. EPR effects cause a 10-fold increase in drug retention when nanoparticles are deployed as delivery vehicles compared with free drug alone [154]. One of the main pivotal factors causing EPR effects is the particle size. A particle size of 100-200 nm results may be optimal for in vivo targeting delivery based on EPR effects.

Active targeting is strictly correlated with passive targeting and occurs only after passive accumulation of the particles within the tumor area. The binding of tumor-

selective ligands to the cognate receptor present on the cell membrane significantly increases nanocarrier intracellular uptake and accumulation into cancer cells [154].

Several type of nanoparticles have been investigate as drug carriers including liposomes, dendrimers, gold nanoshells, nucleid acid-based nanoparticles, and polymeric nanocarriers [155].

1.5.2 Polymeric nanoparticles

Polymeric nanoparticles (PNPs) are versatile carriers able to vehicle small molecules such as drugs or macromolecules such as nucleic acids and proteins [155]. Due to their chemical properties PNPs are able to enter in the cells, to elude degradative system by endosomal escaping once endocited into the cytoplasm and to be stable in the blood stream and prevent the release of embedded molecules leading low toxicity [156, 157, 158]. Currently, PNPs are commonly used for targeting therapeutic molecules to tumor cells.

Polymeric vectors can be synthesized using different materials such as Polylactides (PLA), Polyglycolides (PGA), Poly(D,Llactic-co-glycolides) acid (PLGA), Polyanhydrides, Polyorthoesters, Polycyanoacrylates, Polyalkylcyanoacrylate, Polycaprolactone [155, 159].

In particular, Poly(lactic-co-glycolic acid)-block-poly(ethylene glycol)-carboxylic acid, (PLGA-b-PEG) block-copolymer is emerging as one of the most promising system for nanoparticles formation, drug loading and in vivo drug delivery applications. PLGA-b-PEG is an amphiphilic polymer: the two polymer portions self-assemble during micelles formation, generating a targetable system (due to the presence of a COOH) in which the hydrophobic PLGA remains inside the micelles and the hydrophilic PEG goes outside creating a stabilizing shell. PEG- and PLGA- based polymers are known to be non-toxic GRAS (Generally Recognized As Safe) and FDA-approved [160, 161].

Due to their tunable characteristics, controlled- and sustained-release properties, biodegradability and biocompatibility, polymeric PNPs represent a good strategy for the delivery of drug and/or diagnostic agents. PLGA-b-PEG copolymer has gained large attention in the past decade, since its approval by Food and Drug

Administration (FDA) for biomedical usage due to its ability to create micelles-like nanocarriers displaying an internal hydrophobic PLGA portion, suitable for entrapping lipophilic molecules, and an external hydrophilic PEG forming a stabilizing shell and increasing the half-life of the nanocarrier [160]. PLGA nanoparticles, which are typically 100-200 nm in diameter, even if locally administered by convectional enhanced delivery (CED), have limited mobility and diffusion by convection through the brain interstitial spaces [162,163], which are 38-64 nm in normal brain but show a superior mobility in tumoral regions in which the interstitial spaces is 70-100 nm [150,164].

1.5.3 Chlorotoxin

As mentioned before, nanovectors external layer, can be modified adding different molecules and among them even peptides that give to nanocarriers target specificity. One of the known peptides that target GBM cells is chlorotoxin (CTX). CTX is a 36-residue peptide (MCMPCFTTDHQMARKCDDCCGGKGRGKCYGPWLCR-NH_2) [165] originally isolated from scorpio Leiurus quinquestriatus venom. CTX specifically and selectively binds to GBM cells [166,167] by recognizing its target molecules MMP2 [76] and ClC-3 [168, 169], both abundantly expressed in glioma cells. MMP2 and ClC-3 can constitute a protein complex which is recognized by CTX; the bind of CTX with the MMP2/ClC-3 protein complex inhibit glioma cell invasion ability by inducing their endocytosis [76,169].

2 Materials and methods

SYNTHESIS AND CHARACTERIZATION OF AG-PNP-CTX NANOVECTORS

100 mg of PLGA-b-PEG-COOH (7 kDa-3 kDa) and AgNPs-1, both prepared as already reported 30, were admixed into 10 mL of dimethylformamide (DMF). This organic phase was mixed with 100 mL of ultrapure water under vigorous stirring, maintaining water/organic ratio 10/1 with a constant removal of the solution. The mixture was kept for 30 min. under vigorous stirring then washed and concentrated by using centrifugal filter devices (Amicon Ultra, Ultracell membrane with 100.000 NMWL, Millipore, USA) to a final volume of 5 mL and finally filtered by using a syringe filters phenex-PES of polyether sulfone (26 mm, 0.20 µm, Phenomenex, Italy). To a suspension of the so obtained Ag-PNP (5 mL) in PBS (10 mL, 0.01 M), under magnetic stirring, a solution of N-hydroxysulfosuccinimide 2.3 mM (8.7 mL) and a solution of 1-ethyl-3-(3-dimethylaminopropyl) carbodiimide 0.28 M (3.6 mL) was added. The reaction was carried out at room temperature for 15 minutes then 50 µg of Chlorotoxin, dissolved into 1 mL of water, were added and left to react for 24 hours. After that Ag-PNP-CTX were purified and concentrated to a final volume of 5 mL as previously described. Dynamic light scattering (DLS) analysis and ζ-potential values were obtained with a Zetasizer Nano-S (Malvern) instrument, working with a 532 nm laser beam at 25 °C, using standard cuvettes or DTS1060C Clear Disposable zeta cells, and the results expressed as average of three measurements. Atomic absorption analysis was conducted in a SpectraAA 100 Varian instrument, with opportune AgNO3 standards for calibration line. Final concentration of the suspensions was determined by gravimetric analysis by drying 100 µL of solution at 130 °C for 24 hours then accurately weighting the residual dry matter amount.

CELL CULTURE

Human-derived GBM cell line were grown in Minimum Essential Medium Eagle, Alpha Modification (αMEM) (U87MG) or RPMI (A172, T98G) (Lonza, Basel, Switzerland) supplemented with 10% fetal calf serum (FCS, U.S. Origin, Gibco/Life Technologies), 100 U/ml penicillin and 0,1 mg/ml streptomycin. Cells were mantained at 37°C in a humidified incubator with 5% CO2.

COMPETITIVE INHIBITION ASSAY

U87MG and A172 cell lines were pre-treated for 2 hours with decreasing concentrations of the native CTX peptide (MCMPCFTTDHQMARKCDDCCGGKGRGKCYGPQCLCR-NH_2) (H6086, Bachem, Bubendorf, Switzerland) followed by incubation with targeted (Ag-PNP-CTX) or non-targeted (Ag-PNP) nanovectors at Ag concentration of 100 μM for 16-18 hours (overnight). The intracellular accumulation of Ag nanoparticles (Ag-nps) was determined by confocal laser scanning microsco and 3D imaging analysis performed by IMARIS software (see below).

MOUSE ORTHOTOPIC XENOGRAFTS

Mouse experiments were carried out according to the protocol approved by Italian Minister of Health (protocol number 171/2013-B). CD-1 male nude mice, 6-8 weeks (Charles Rivers Laboratories, Calco, Italy) were housed in specific pathogen free animal house. Sterilized Water and rodent chow were given ad libitum. Mice were injected intracranially into the right striatum with U87MG cells at $5x10^4$ cells/mouse or luciferase-transfected U87MGluc2 (gently provided by Laura Cerchia, CNR Naples, Italy) 10^5 cells/mouse. For intra-tumor nanovector accumulation analysis and quantification, U87MG-tumors were allowed to grow for 15 days, and then mice were subject to whole-brain single dose radiation (2 Gy). Ag-PNP-CTX were administered intraperitoneally at a dose of 1mg of dry matter 18 hours after radiations. Animals were euthanized 24 or 48 hours after nanovector injection. For immunofluorescence experiments intracardiac perfusion was carried out with 4% PFA. The harvested brains and organs were frozen and conserve at -80°C.

To study the antitumor effect of Ag-PNP-CTX, U87MGluc2-tumors were allowed to growth for 11 days, and then mice were randomized and divided in 4 groups: not treated animals (controls), animal treated only with Ag-PNP-CTX nanovectors, animal treated only with radiations, and animal treated with radiations and Ag-PNP-CTX nanovectors. Mice were subject to whole-brain single dose radiation (2 Gy, T0). Ag-PNP-CTX administration started 18 hours after radiation treatment. Mice received 4 consecutive doses of Ag-PNP-CTX nanovectors (first 2 doses: 1 mg of dry matter; third and fourth doses: 0,5 mg of dry matter) at intervals of 48-72 hours.

IN VIVO IMAGING OF INTRACRANIAL TUMORS

An IVIS II Imaging System (Caliper LifeScinces- Perkin Elmer-Waltham, Massachusetts, USA) was used to take photograph and luminescent images setting an open filter and binning 8. Exposure time was fixed at 1 minute and 5-10 images were acquired until maximum photon flux achievement. Ten minutes before acquisition, mice were administered intraperitoneal injection of D-luciferin (Perkin Elmer-Waltham), 150 mg/Kg, as a substrate for the luciferase enzyme. Images were captured and quantified with Living Image 4.3.1 software (Perkin Elmer-Waltham), based on equivalent regions of interest over the head. Analysis was carried out using the Living imaging software (Perkin Elmer - Waltham, Massachusetts, USA) setting binning 4 and “automatic ROI” (thershold 50%) for all images.

RADIATION TREATMENT

Cells and mice were irradiated with a single dose of 2 Gy using an x-ray biological irradiator operating at 12 mA/190 kv (RADGIL, Gilardoni, Lecco, Italy). Cells were irradiated at a dose rate of 0,65 Gy/min. Mice were irradiated at a dose rate of 0,4 Gy/min in an in-house designed lead irradiation jig that allowed only the head to be exposed and shielded the body.

IN VITRO NANOVECTOR INTRACELLULAR UPTAKE

U87MG, A172, T98G were seeded on glass cover slips (16 mm diameter) at a density of 15.000 cells/coverslip in the presence of 5% FCS. After 24h of culture, the cells were incubated with targeted (Ag-PNP-CTX) or non-targeted (Ag-PNP)

nanovectors at Ag concentration of 100 μM for 16-18 hours (overnight). One hour before cell fixation, Syto Blue 45® fluorescent dye (Life Technologies Corporation, Carlsbad, Ca, USA) was added to the medium (1:1000). After three washes in Dulbecco's Phosphate Buffered Saline (PBS) (Sigma-Aldrich, St. Louis,MO, USA), cells were fixed in 4% paraformaldehyde for 15 min at room temperature. Glasses were mounted with a PBS/Glicerol (Sigma-Aldrich, St. Louis, MO, USA), mixture (1:1) added with DAPI (Sigma-Aldrich, St. Louis, MO, USA), fluorescent stain 1:40.000.

IMMUNOSTAINING

Before immunostaining fixed 10-micron-thick frozen brain section were heat antigen retrieved in Sodium Citrate (pH=6). Unspecific binding was blocked with 10% horse serum (Sigma) diluted in PBS/Triton 0,1% (1 hour). Primary antibodies against human-nestin clone 2C1.3A11 (1:250 1h RT) (Abcam), human-MMP-2 (1:100 1h RT) (Sigma/Prestige Antibodies), human-ClCN3 (1:100 1h RT) (Cell Signaling Technology, Beverly, MA,USA), human-LAMP1 (BD Bioscience) (1:100 1h RT) and mouse-claudin-5 (1:600 24h 4°C) (Millipore) were employed at same experimental conditions for both cell lines and brain cryosections. After primary antibody, samples were incubated with the appropriate secondary antibodies conjugated with one of the indicated fluorophores, Alexa fluor: 488, 555, 561 (Invitrogen) (dilution 1:200; 1 hour RT). Early endosome were marked using Cell Light Early Endosome-RFP, BacMan 2.0 (Invitrogen) according to the procedure instruction.

TUNEL ASSAY

Detection of apoptosis was carried out by in situ TUNEL-assay (Click-iT® TUNEL Alexa Fluor® 633 Invitrogen-Life Technologies, Grand Island, NY, USA). TUNEL was performed according to the protocol provided by the manufacturer. Briefly, after slide incubation (10 minutes at 37°C) in TdT reaction buffer, samples were incubated with TdT reaction mixture for 60 minutes at 37°C. After washes with PBS1x sections were washed with 3% BSA and 0.1% Triton® X-100 in PBS for 5 minutes. The Click-iT® Plus TUNEL reaction cocktail was added to each slide for 30 minutes at 37°C.

CONFOCAL MICROSCOPY AND IMAGES ANALYSIS

Confocal microscopy was performed using a Leica TCS SP5 confocal microscope equipped with a resonant scanner (scan speed 8000 Hz) and a HCX PL APO 63x/1.4 OIL objective, a HC PL FLUOTAR 10.0x0.30 DRY and a HC PL FLUOTAR 20.0x0.50 DRY. Ag-nanoparticles (nps) were acquired in reflection mode upon 458 nm excitation for in vitro cell experiments and upon 488nm excitation for in vivo experiments on brain cryosections. Syto blue was excited by the 458 nm laser line, nestin and phalloidin by the 488 nm line of an Argon laser, claudin, MMP-2 and ClC-3 by the 561 nm laser line of a diode laser. Voxel size was established using Nyquist criteria.

Intracellular Ag-nps quantification was carried out by 3D imaging analysis by means of IMARIS software (Bitplane, IMARIS) using the "Cells" function and the following set-up: cell detection/smooth filter =0,160; Background Subtraction, sphere diameter=20; Detect Vesicles, Estimated Diameter= 240 nm; Vesicle Quality=18).

Ag uptake analysis in vivo was performed using IMARIS software using the "Spots" function into a fixed area (6500 μm2) for all fields, murine or human xenograft sites.

MMP-2 and CLC-3 levels expression analysis was performed using Image J software. In brief, the central, the upper and the lower section of a 6 μm z-stack was analyzed for each image. MMP-2 and ClC-3 Threshold mask was kept constant and using the tool "Analyze Particles" area of MMP-2 and ClC-3 signal was calculated. MMP-2 and ClC-3 area was normalized on number of nuclei present in the slice analyzed.

WESTERN BLOTTING

Approximately $2x10^5$ U87MG cells were lysed in ice-cold lysis buffer (100 mM Hepes, 2mM EDTA, 1% SDS) supplemented with protease inhibitors (ROCHE) and then stored at −80°C until used. Protein concentrations were determined using a BCA protein assay (Pierce). Equal amounts of protein (20 μg) were loaded on 10% polyacrylamide gels and resolved on SDS-PAGE. Membranes were blocked (1 hour RT) with 5% milk in PBS/tween-20 0,1% (Sigma) and then probed (1 hour RT) with anti-human MMP-2 polyclonal rabbit antibody (1:1000) (Sigma), anti-human ClC-3

monoclonal rabbit antibody (1:1000) (Cell Signaling Technology, Beverly, MA,USA) and anti-human β–actin monoclonal mouse antibody (1:5000) (Sigma). Anti-rabbit and anti-mouse HRP-conjugated secondary antibodies (Pierce, Rockford, IL, USA) were employed at a dilution of 1:5000 for 1 RT. Bands were visualized by Bio-Rad Clarity western ECL substrate (Biorad, Hercules, USA), and detected by ChemiDoc MP system (Biorad, Hercules, USA). All densitometric analyses were carried out using Image Lab software version 5.1 (Biorad Hercules, USA).

GELATIN ZYMOGRAPHY

Supernatant from in vitro grown U87MG cells were eluted in Zymogram Sample Buffer (Biorad, Hercules, USA) according to producer instructions. Equal amount of each samples were loaded in Ready Gel® Zymogram Precast Gels (Biorad, Hercules, USA) and electrophoresis was carried out at fixed voltage of 90 V. The gels were washed twice in distilled water for 10' and twice in Zymogram Renaturation Buffer (Biorad, Hercules, USA) for 30' and then incubated for 6 hours at 37°C in Zymogram Development Buffer (Biorad, Hercules, USA). After incubation, gels were stained with Bio-Safe Coomassie Stain (Biorad, Hercules, USA) for 2 hours. Gelatinolytic activity was detected as transparent bands on a blue background. Images were acquired with chemidoc system (Biorad, Hercules, USA). Densitometry analysis was performed with ImageJ Software.

MTT ASSAY

U87MG cells (5,000 cells/well) were plated in 96-well plates with 100 µl αMEM medium. After 24 h cells were treated with increasing concentrations of Ag-nps encapsulated in the PNP nanovectors, whereas no treatment was done as positive proliferation control. At 72 h, 25 µl of 5 mg/ml 3-(4,5-dimethylthiazol-2-yl)-2,5-diphenyltetrazolium bromide (MTT, Sigma-Aldrich, St Louis, MO) was added directly to the cells followed by an additional 4 hours of incubation, then 100 µL of DMSO was added. The optical density of individual wells was measured at a wavelength of 550 nm with the Sunrise apparatus (Tecan Group, Ltd, Mannedorf, Switzerland). All assays were performed in triplicate.

STATISTICS

Data are presented as mean ± SE. If not indicated mean values were compared by the Student's t test (two-tailed, non parametric). Statistics and fitting of experimental data were performed with Graph Pad Prism6.

3 Aim of the project

Glioblastoma (GBM) is still an incurable disease, with a life expectancy of around 14 months from the diagnosis. The cause of this negative prognosis is due to various factors including the presence of GBM staminal cells, and the high grade of invasivity, drugs resistance and recidivism. Another important factor leading to drugs failure is related to the anatomical position in which tumor develops: the brain. Brain vasculature is characterized by the presence of the BBB, which contributes to significantly impeding chemotherapics from reaching malignant cells scattered in the brain parenchyma. Niches of GBM cells can thus grow and lead to recidivism. So far, any treatment is ineffective in case of recidivism, and the impossibility of totally eradicating GBM with the current clinical approaches is a powerful motivation to trying to devise new strategies. Under this respect, nanotechnological devices (especially nanoparticles), have been suggested as innovative tools for the therapy and diagnosis of central nervous system diseases by increasing drug accumulation in cells and escaping the efflux mechanisms. Aim of this work was the assessment of the effectiveness of polymeric nanovectors, combined with radiotherapy, in reaching GBM tumor cells, in particular those in the peripheral tumor niches, and determining tumor growth inhibition. With the intent to quantify targeted nanovectors reaching tumor cells, and to track their localization, PLGA-*b*-PEG nanovectors conjugated to Chlorotoxin (CTX) and encapsulating silver nanoparticles (Ag-nps), visible with optical and confocal microscope imaging in reflection mode (Ag-PNP-CTX), were employed.

Specific goals were to evaluate:

- Tumor-specific intracellular uptake, intracellular trafficking and endosomal escape of Ag-PNP-CTX nanovectors, with and without the radiation treatment.

- Ag-PNP-CTX nanovector quantification and biodistribution in the tumor, in the brain parenchyma, and in the peripheral organs after systemic administration in U87MG orthotopic xenografted mice.
- The in vivo effects of ionizing radiations on the Ag-PNP-CTX distribution in the U87MG-tumor microenvironment and brain parenchyma.
- The in vivo evaluation of synergistic therapeutic effect of radiations and Ag-PNP-CTX nanovectors concomitantly administered.

4 Results

4.1 Synthesis and Characterization of Ag-PNP-CTX nanovectors

In order to assess the efficacy of polymeric nanocarriers to target GBM cells, poly (lactic)-co-glycolic)-co-poly ethylene glycol (PLGA-b-PEG) nanovectors (PNPs) conjugated to CTX (PNP-CTX) and encapsulating silver nanoparticles (Ag-nps) have been synthesized.

Ag-PNP-CTX were prepared by Prof. Mauro Comes Franchini (Department of Industrial Chemistry "Toso Montanari", University of Bologna, Italy.) following a procedure already reported by Locatelli et al. 2012 (Figure 7 A) [170]. Firstly, Ag-nps were obtained through reduction of AgNO3 by glucose and NaOH in presence of polyvinylpyrrolidone (PVP) and later they were coated with the organic ligand 1 in order to obtain lipophilic nanoparticles (Ag-nps-1) [171]. Native Ag-nps present a hydrodynamic diameter of 35.4 ± 5.3 nm, which increased to 40 ± 7.6 nm after the coating with the organic ligand. A complete characterization of Ag-nps-1 was previously reported [172].

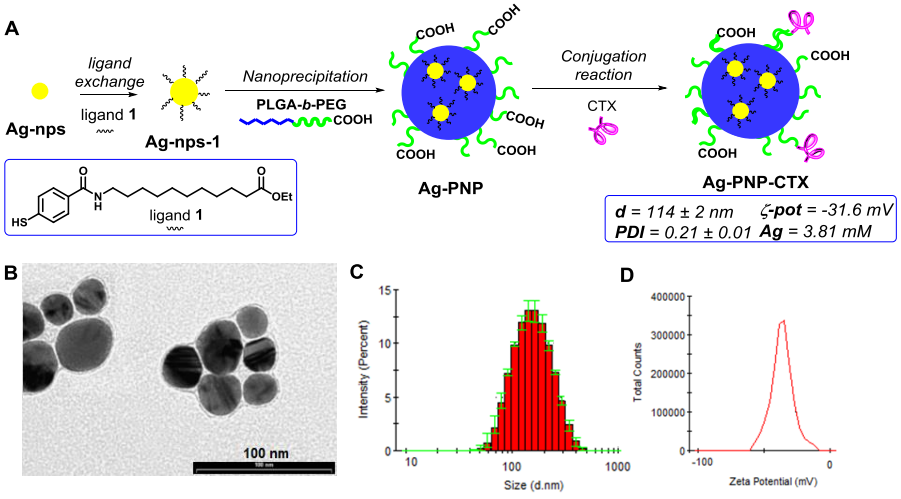

Figure 7. (A) Schematic procedure for the synthesis of Ag-PNP-CTX. Representative TEM image (B) DLS analysis (C) and ζ-potential analysis (D) of Ag-

The nanoprecipitation method was exploited for this purpose and led to the entrapped of Ag-nps-1 in the inner core of the water-soluble PNP. Ag-PNP were then chemically conjugated onto the outer shell with the specific targeting agent CTX, thus giving Ag-PNP-CTX (Figure 7A). For this reaction the presence of carboxylic acid groups, derived from PEG chains, onto the surface of Ag-PNP was exploited for the formation of an amide bond with free-amino ending group of CTX absorption spectroscopy (AAS). PNP-CTX were characterized by Transmission Electron Microscopy (TEM, Figure 7B). Dynamic light scattering (DLS) revealed particles with diameter equal to 114 ± 2 nm, a low polydispersity index (PDI) (0.21 ± 0.01) (Figure 7C) and a negative ζ-potential (-31.6 mV) (Figure 7D). Silver concentration was determined to be 3.81 mM by means of atomic Ag-nps-1 were then entrapped into PLGA-PEG polymeric nanoparticles (PNP). The overall Ag-PNP-CTX concentration was established by gravimetric analysis and found to be 8.87 mg/mL.

4.2 Optical imaging and quantification of encapsulated Ag-nps

The use of Ag-nps has enabled us the use of confocal microscopy to visualize and quantify CTX-targeted nanovectors. The laser set in reflectant mode allowed Ag-nps detection (Figure 8 B). By means of this strategy, the cytoplasmatic amount of polymeric nanovectors has been quantified in 3 different human GBM-derived cell lines (U87MG, A172 and, T98G) after over-night incubation.

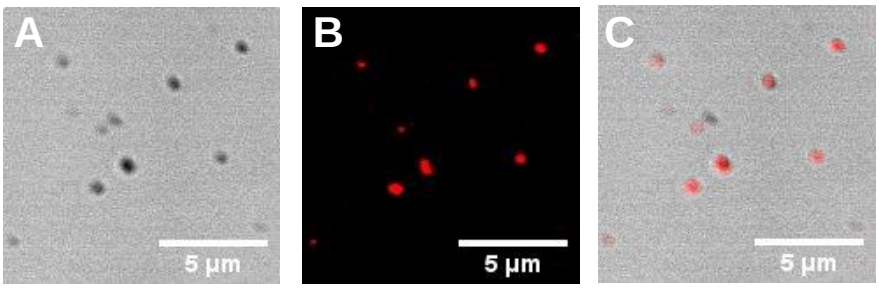

Figure 8. Ag detection under laser reflection mode. (A-C) Pictures of Ag-nps: (A) bright field, (B) reflection mode (C) merge. Metal Ag-nps have been acquired in reflection mode upon 458 nm excitation and are shown in red.

In order to evaluate the tumor specific binding CTX-mediated, the amount of intake of functionalized nanovectors has been compared with not functionalized ones.
Data on the exposure of CTX-functionalized and non-functionalized nanoparticles to the 3 GBM cell lines show that CTX is able to significantly increase PNPs uptake (Figure 9 A-E).

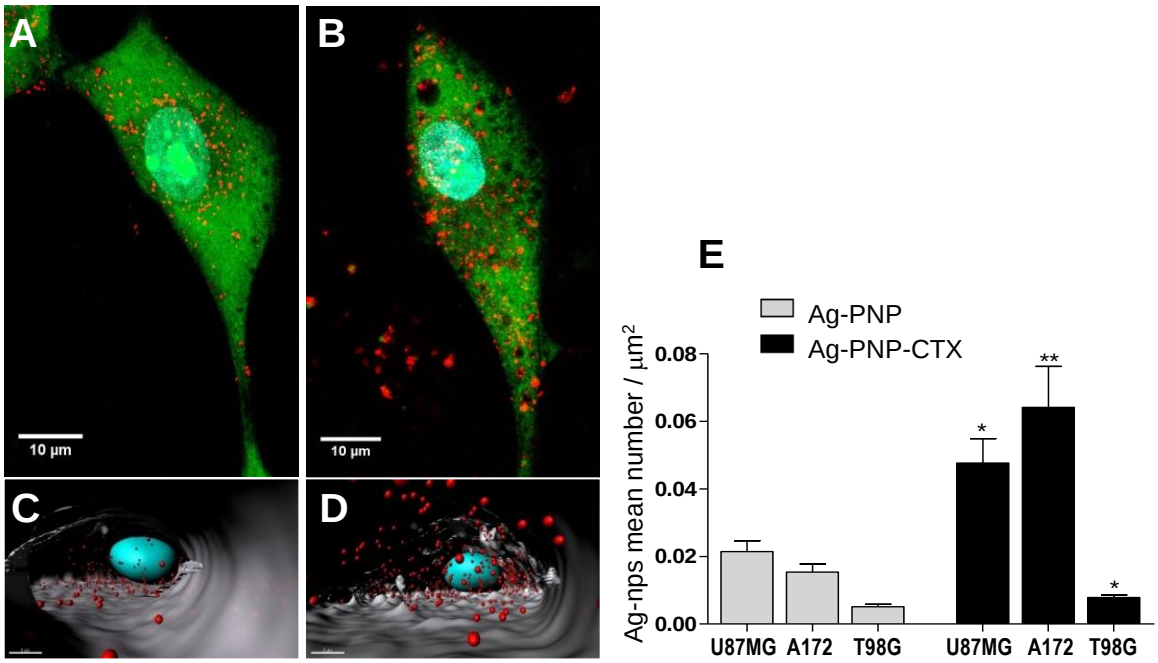

Figure 9. Human-derived GBM cell lines U87MG, A172 and T98G were incubated o/n in the presence of targeted (Ag-PNP-CTX) or non-targeted (Ag-PNP) nanovectors at Ag concentration of 100 µM. The intracellular accumulation of Ag nanoparticles (Ag-nps) was determined by confocal laser scanning microscopy (A, B) and 3D imaging analysis performed by IMARIS software (C and D). (A) and (B) images represent the maximum projections of 20 optical sections of the cell labelled with Syto Blue 45® (green). Metal Ag-nps have been acquired in reflection mode upon 458 nm excitation and are shown in red and DAPI signal for nuclei detection in blue. (C) and (D) computation 3D images of the peri-nuclear region of cells in panel A and B respectively. (E) Intracellular Ag-nps quantification expressed as mean number of Ag-nps ± ES normalized on the cell surface (mm2). About 60 cells / experimental group from 2 or 3 independent experiments were analyzed. Significance versus cells incubated with non-targeted nanovector (Ag-PNP): * p<0,02; **p<0,005.

To exclude a CTX conformational change due to its binding to the polymeric core which could prevent CTX binding to its targets (MMP2 and ClC-3), a competitive assay has been carried out. The competition test was performed by pretreating GBM cells with increasing concentrations of native CTX peptide (from 500 ng to 1 ng/ml). Results showed a significantly lower, dose-dependent, PNPs uptake when cells were

incubated in the presence of native CTX peptide and CTX functionalized nanovectors. On the contrary, CTX native peptide did not modify the cellular uptake of non-targeted Ag-PNP nanovectors (Figure 10). These results strongly suggest that the covalent interaction between polymeric nanocarriers and CTX does not interfere with the ability of the peptide in recognizing its targets.

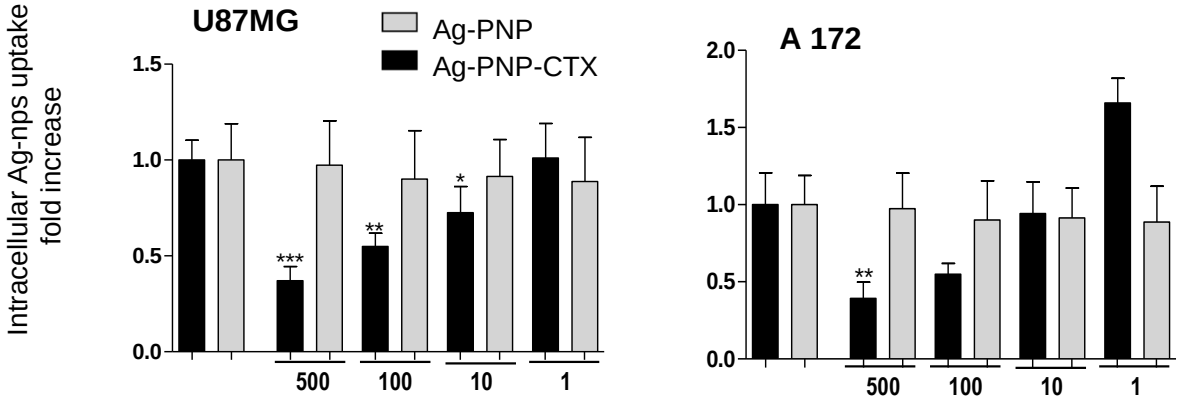

Figure 10. Competitivity assay. Competitive inhibition of cellular uptake of Ag-PNP-CTX and Ag-PNP nanovectors in U87MG and A172 cells incubated with native CTX peptide at the indicated concentrations (ng/ml). Results are expressed as Ag-nps quantity ± ES normalized to the Ag-nps detected in cells incubated without native CTX peptide (first columns). Significance versus cells incubated in the absence of CTX peptide: U87MG * p=0,0334 ** p=0,0057 *** p=0,0004; A 172 ** p=0,0052.

Therefore, the result of the competitivity assay can reasonably lead one to suppose that Ag-PNP-CTX endocytosis is a receptor mediated process. This type of endocytosis converges in endosomal/lysosomal pathway [173]. In order to assess the Ag-PNP-CTX ability to escape from endosomal compartment, the intracellular trafficking has been analyzed.

Qualitative analysis showed no co-localization of Ag-nps with endosomal and lysosomal fluorescent markers (Figure 11) implying that CTX-nanovector cargo would be entirely released into the cytoplasm and not sequestered and/or degraded inside cellular organelles

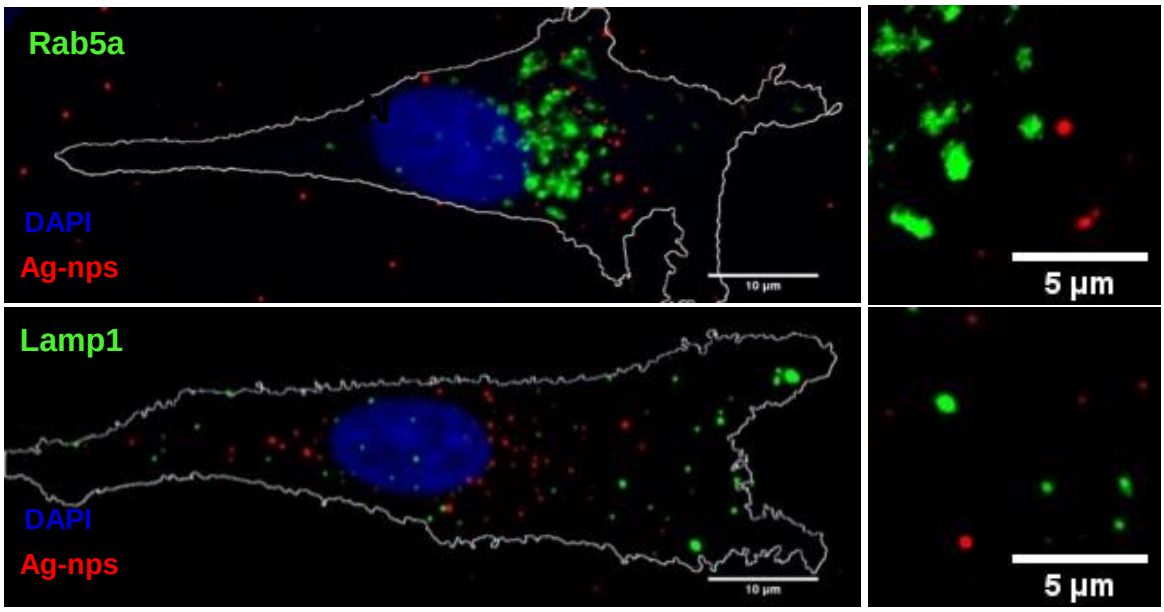

Figure 11. Representative confocal microscopy images of single central plane of the whole z stack showing U87-MG cells incubated in the presence of Ag-PNP-CTX nanovectors. Intracellular endosomal and lysosomal compartments were identified using the specific-associated markers Rab5a and LAMP-1 respectively.

4.3 Radiations promote CTX-functionalized nanovectors accumulation in GBM tumors

The in vivo tumor distribution of Ag-PNP-CTX nanovectors was evaluated in an orthotopic murine model of GBM. By means of stereotactic techniques, human U87MG has been transplanted in the right striatum of nude mice, one of the brain region in which GBM most frequently arise. To increase the infiltrative capacity, 7-10 days before brain transplantation U87MG cells were grown in α MEM medium and low serum concentration (5% serum). Using an antibody directed against human nestin, a staminal marker overexpressed in glioma stem cells [174], it has been possible to distinguish human GBM cells from murine sourrounding cells (Figure 12). After 15 days from tumor transplantation, it has been possible to detect a relevant “central” tumor mass (figure 12 A) and infiltrative tumor niches within the healthy parenchyma at the periphery of the tumor (Figure 12 B). Outstandingly, it has been possible to detect single tumor cells spread into healthy tissue (Figure 12 C). In order to evaluate the amount of Ag-PNP-CTX able to reach the tumor, a single dose of

PNPs has been administered intraperitoneally; after 20 hours from PNPs injection it has been possible to evaluate the presence of Ag-PNP-CTX at the tumor level. Similarly to in vitro, in vivo Ag-nps have been detected by confocal microscopy with the laser set in reflection mode. Quantification of Ag-nps carried out on brain cryosections showed a significantly higher level of accumulation in the GBM-tumor compared to healthy brain parenchyma, resulting in a mean number of Ag-PNP-CTX for each volume analyzed in every imagine (6500 μm^3) amounting to 26,36 (± 3,157 ES) versus 0,7292 (± 0,1528 ES) (Figure 13 B) respectively. After 48h following nanoparticles injection, a wash-out of Ag-PNP-CTX has occurred (Figure 13 B): the mean number of nanoparticles is 7,291 (± 1,598 ES) versus 26, 36 at 24h (Figure 13 B). The wash-out occurs also in the healthy murine portion of cerebral parenchyma, in which the mean number of Ag-PNP-CTX at 48h after injection has been found to be 0,5968 (± 0,1426 ES) (Figure 13 B).

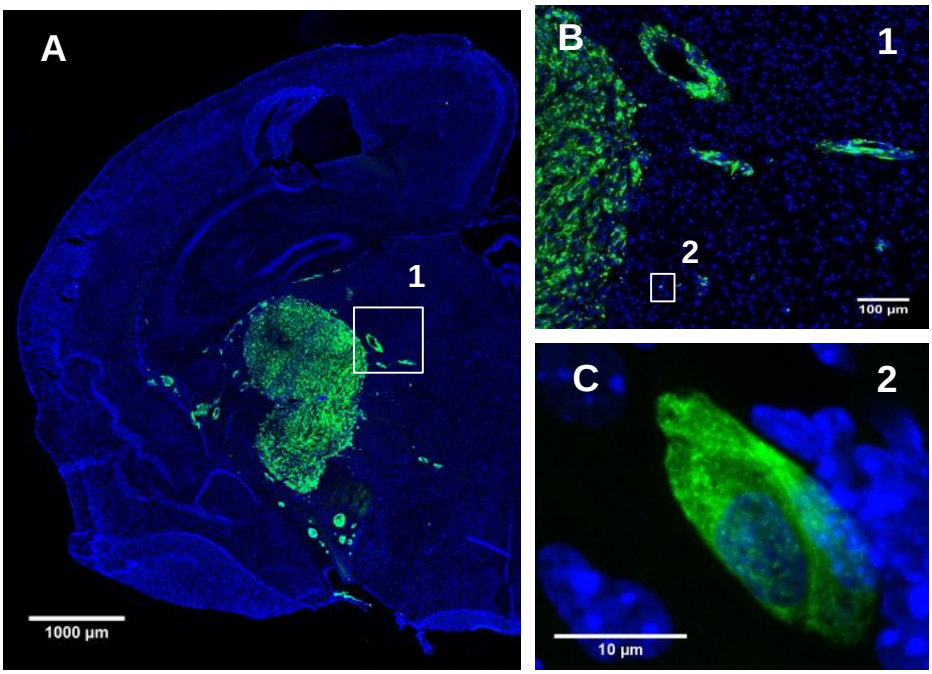

Figure 12. U87MG ($5x10^4$) cells were injected intracerebrally into athymic 6-8 weeks old male mice. After 2 weeks, animals were euthanized with intracardiac perfusion of PBS, followed by formaldehyde. GBM xenografts were detected by immune staining for human nestin (green). In blue is the DAPI signal for nuclei detection. (A) representative coronal section 15 days after tumor implantation; (B) and (C) magnified views of the indicated insets.

In order to mimic, to the greatest possible extent, the clinical conditions in which RT is employed, a radiation treatment was added to the experimental procedures in order to evaluate whether ionizing radiations could modulate Ag-PNP-CTX localization both at the tumor and healthy parenchyma level. A single 2 Gy administration has been performed 18h before Ag-PNP-CTX injection in the whole brain.

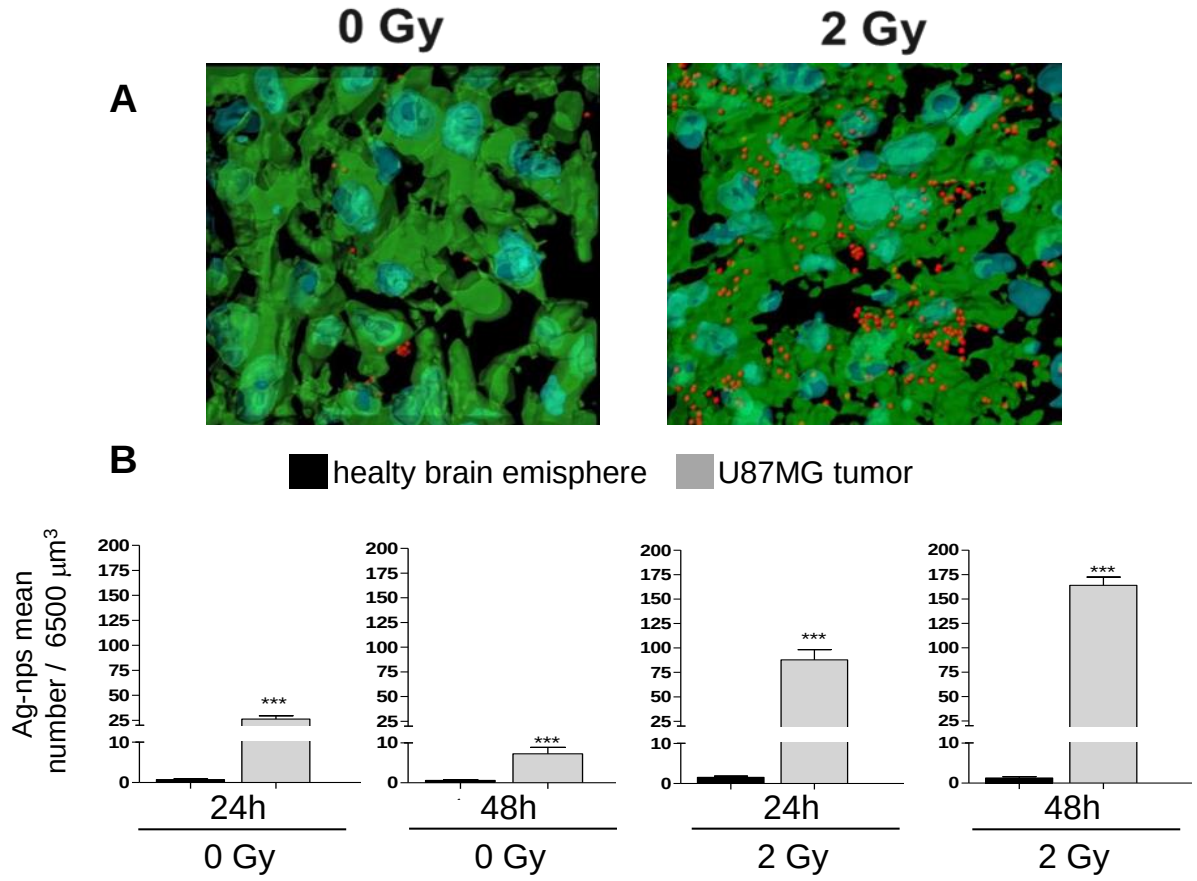

Figure 13. In vivo accumulation of Ag-PNP-CTX nanovectors at tumor site assessed in U87MG orthotopic xenografts model. Fifteen days after implantation of tumor cells mice were subjected to total brain radiation treatment (2Gy). A parallel group of non-irradiated mice (0 Gy) was considered as control. Ag-PNP-CTX were administered intraperitoneally 18 hours after radiations at a dose of 1mg/mouse. Animals were sacrificed 24 or 48 hours after nanovector injection. A) Representative images of renderings of U87MG tumor mass cryosections taken from irradiated (2 Gy) and non-irradiated (0 Gy) mice injected with Ag-PNP-CTX (0Gy). Ag-nps have been acquired in reflection mode upon 488 nm excitation and are shown in red. Green areas show human nestin immunostaining; the nuclei are shown in blue (DAPI). B) Ag-nps quantification was performed in brain cryosections by confocal microscopy and IMARIS 3D imaging analysis.. (B) Ag-nps quantification is expressed as mean number of Ag-nps ± ES in a fixed volume of 6500 μm^3 . About 60 microscopy fields randomly taken from 4 mice in each experimental group were acquired and analyzed. Significance versus healthy brain tissue: ***p<0,0001.

Results from Ag-nps quantification indicated a further, noteworthy increased (about 4 to 6 folds) amount of Ag-nps in U87MG-tumors from mice subjected to radiations compared to U87MG-tumors from non-irradiated mice (Figure 13B). The mean number of Ag-PNP-CTX in tumors irradiated 24h and 48h after nanovector injection amounts to 87,86 (±10,46 ES) versus 163,9 (±8,584 ES) respectively (Figure 13 B). Interestingly, no wash-out of nanovectors has been shown to occur 48h after Ag-PNP-CTX administration, indeed a higher quantity of Ag-nps has been detected compared to 24h after injection. Noteworthy, radiation treatment determined a non-significant increase of Ag-nps accumulation in the healthy brain

4.4 Radiations alter the blood-brain barrier allowing the targeting of GBM cells infiltrating healthy brain parenchyma

Next aims have been to assess whether the lack of Ag-nps in the irradiated brain healthy parenchyma was due to the presence of an intact BBB, and to investigate the contribution of BBB disruption in increasing accumulation of Ag-PNP-CTX nanovectors in GBM tumors observed upon radiation treatment. To this end an immunostaing for Claudin-5, one of the most expressed brain endothelial tight junction proteins contributing to the maintenance of BBB integrity [175], was carried out. Claudin-5 pattern of expression have been determined by immunofluorescence on cryosections from normal and U87MG-implanted brain hemispheres treated and non-treated with radiations. Results indicated that a single dose of 2 Gy radiation caused alterations in claudin-5 distribution pattern, which was particularly evident in the healthy brain where the formation of gaps in brain vessel wall, caused by the opening of the tight junctions, was detectable (Figure 14 B).

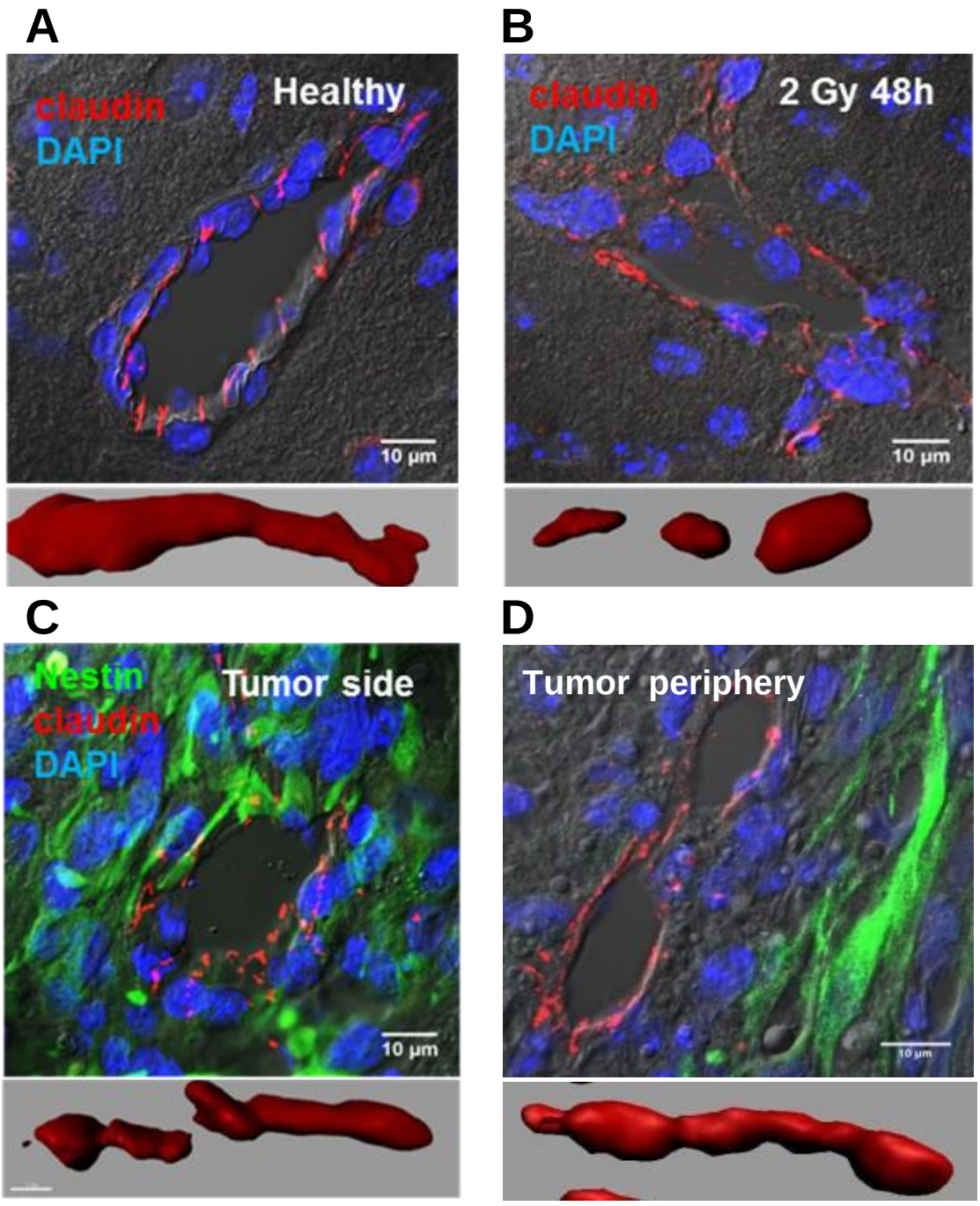

Figure 14. In vivo BBB integrity.(A-D) Confocal images (maximum projections) of normal and tumor-associated blood vessels. Brain cryosections from U87MG-trasplanted mice previously irradiated (2Gy) or non-irradiated (0 Gy) were immunostained for claudin-5 (red) and human nestin (green). Nuclei were revealed by DAPI staining (blue). Lower panels are representative 3D rendering of selected regions of claudin-5 staining carried out by IMARIS software.

In the proximity of the peripheral zone of the tumor we observed a normal claudin-5 expression, suggestive of an intact BBB (Figure 14 D). No Ag-nps accumulation has

been observed in nestin-positive disperse cancer cells (Figure 15, left panel) located far from the tumor mass. After 2 Gy radiation treatment, however, in line with BBB permeabilization, Ag-nps could be detected in the isolated GBM cells branching into the healthy parenchyma (Figure 15, right panel).

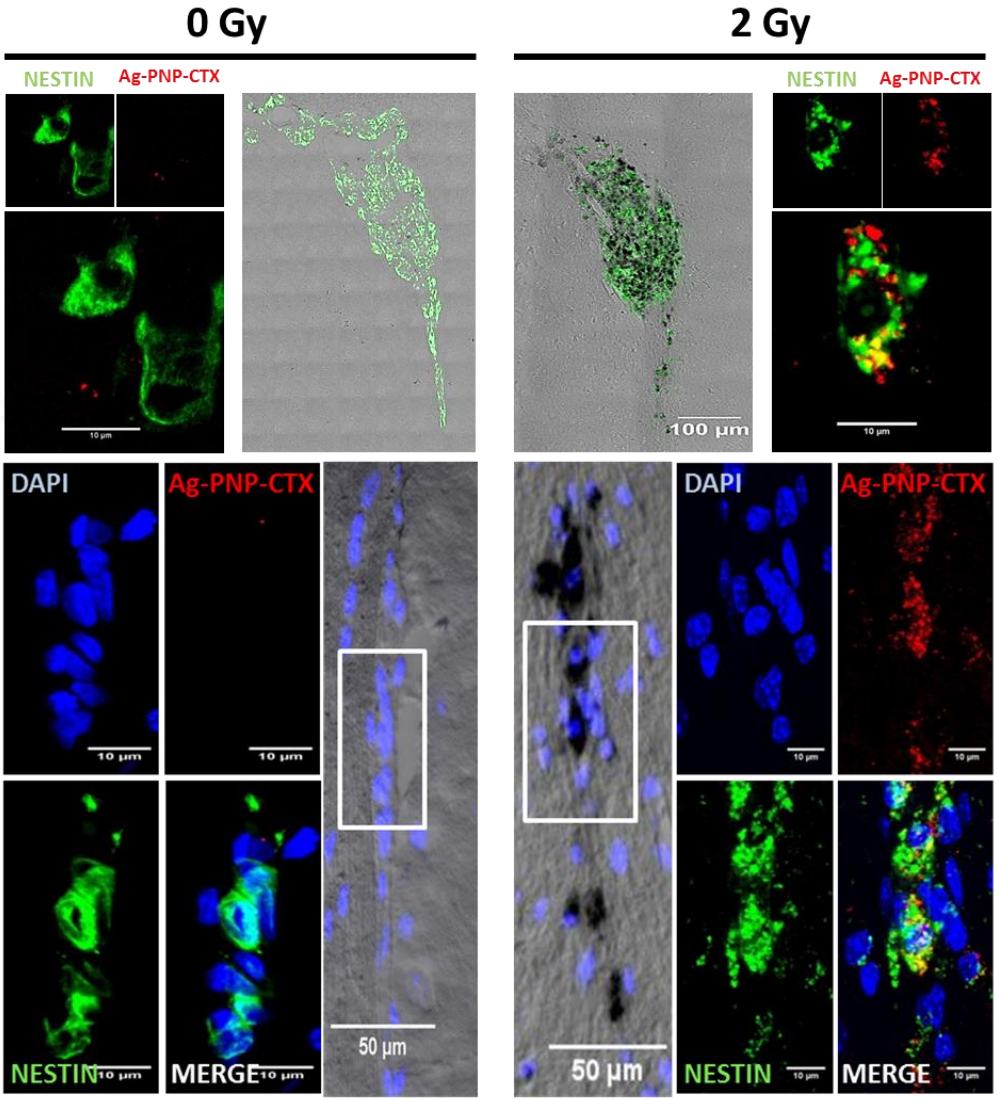

Figure 15. **Ag-PNP-CTX nanovector diffusion in peripheral tumor areas**. Ag-nps and nestin co-localization in single cells present at the U87MG tumor periphery from non-irradiated (0Gy, left panel) and irradiated (2Gy, right panel) mice injected with Ag-PNP-CTX. The isolated cells, labeled with antibodies recognizing human nestin (in green), is a tumor cell which infiltrates the healthy mice tissue, which is negative for the human nestin antibody. In the bright field Ag-nps are visible as black dots. In the lowers panel representative bright field images acquired by differential interference contrast (DIC) of cryosections of non-irradiated (0 Gy) and irradiated (2 Gy) peripheral tumor tissues from U87MG orthotopic xenografts inoculated with Ag-PNP-CTX nanovectors. Ag-nps are visible as black spots. Lateral panels are magnified views of the indicated insets. Ag-nps have been acquired in reflection mode upon 488 nm excitation and are shown in red.

4.5 Radiation Augments Specific Cellular Uptake and Intracellular Localization by inducing MMP-2 and ClC-3 overexpression

In order to understand the effective role of x rays on increasing Ag-PNP-CTX in GBM cells, in vitro experiments have been carried out. The amount of PNPs has been evaluated after a single dose of 2 Gy on two human GBM cell lines, U87MG and T98G.

Notably, while irradiated cells, both U87MG and T98G lines, incubated in the presence of Ag-PNP-CTX displayed a significant increase in intracellular Ag-nps, no variations were observed in either cell lines when incubated in the presence of non-targeted Ag-PNP nanovectors (Figure 16 A and 16 B). Given that CTX is the ligand for MMP-2 and ClC-3, which are highly expressed in human gliomas [166,169], the expression level of these molecules in non-irradiated and irradiated was compared. RT is known to induce MMP-2 expression [176-178] but no data are available yet on ClC-3 expression after radiation treatment.

Western-blot results showed an up-regulation of MMP-2 and ClC-3 levels of expression induced by radiations (Figure 16 B). The effect was particularly evident for CIC-3. Similarly, simultaneous microscopy detection of MMP-2 or ClC-3 and Ag-nps in non-irradiated and irradiated U87MG cells confirmed that radiations increase MMP-2 and ClC-3 levels of expression, which correlate with a higher amount of internalized Ag-nps (Figure 16 A and D).

Notably, the increased expression of MMP-2 and ClC-3 was observed also in vivo, in irradiated U87MG xenografts (Figure 17).

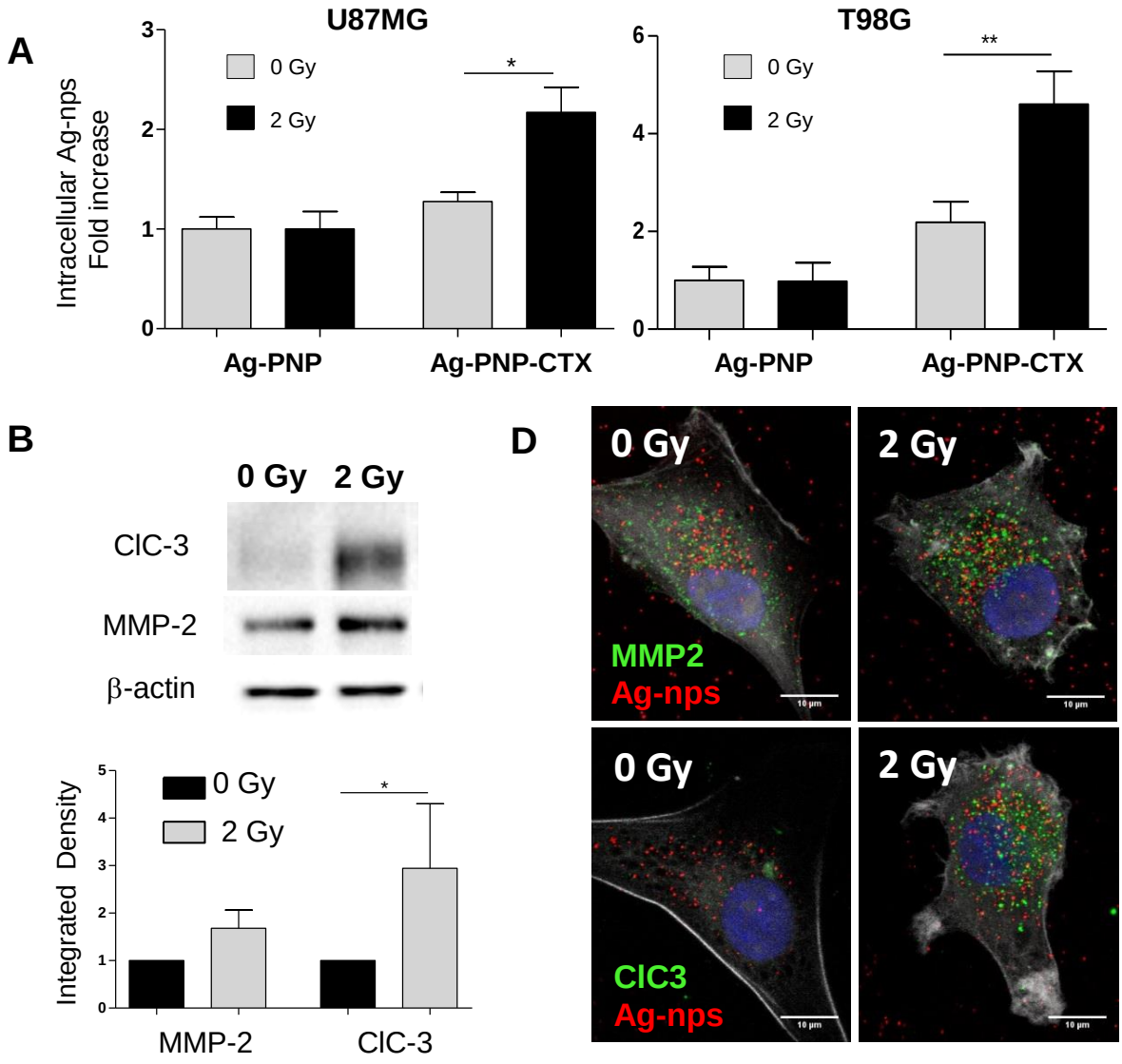

Figure 16. Radiation induced CTX-nanovector intracellular uptake, MMP-2 and ClC-3 expression. (A) Intracellular Ag-nps quantification in irradiated (2 Gy) and non-irradiated (0 Gy) U87MG or TG98 cells incubated overnight in the presence of Ag-PNP or Ag-PNP-CTX. Results are expressed as Ag-nps quantity ± ES normalized to the Ag-nps detected in non-irradiated cells incubated with Ag-PNP(0 Gy Ag-PNP, first column). For analysis details see also Supplementary figure 1. Significance versus non-irradiated cells: * p=0,0117. (B) Western-blot analysis of MMP-2 and ClC-3 expression in irradiated and non-irradiated U87MG cells. One representative experiment out of 4 performed is reported. Levels of β-actin are reported as control for protein loading. (C) Densitometry analysis of western-blot bands (panel B) performed by Image-Lab software. Results normalized on corresponding β-actin. (D) Ag-nps (red) and MMP-2 or ClC-3 (green) signals in irradiated (2Gy) and non-irradiated (0 Gy) U87MG cells shown as maximum projections of 6 optical sections. In blue is the nuclear staining (DAPI). Cell borders were defined by phalloidin staining (gray).

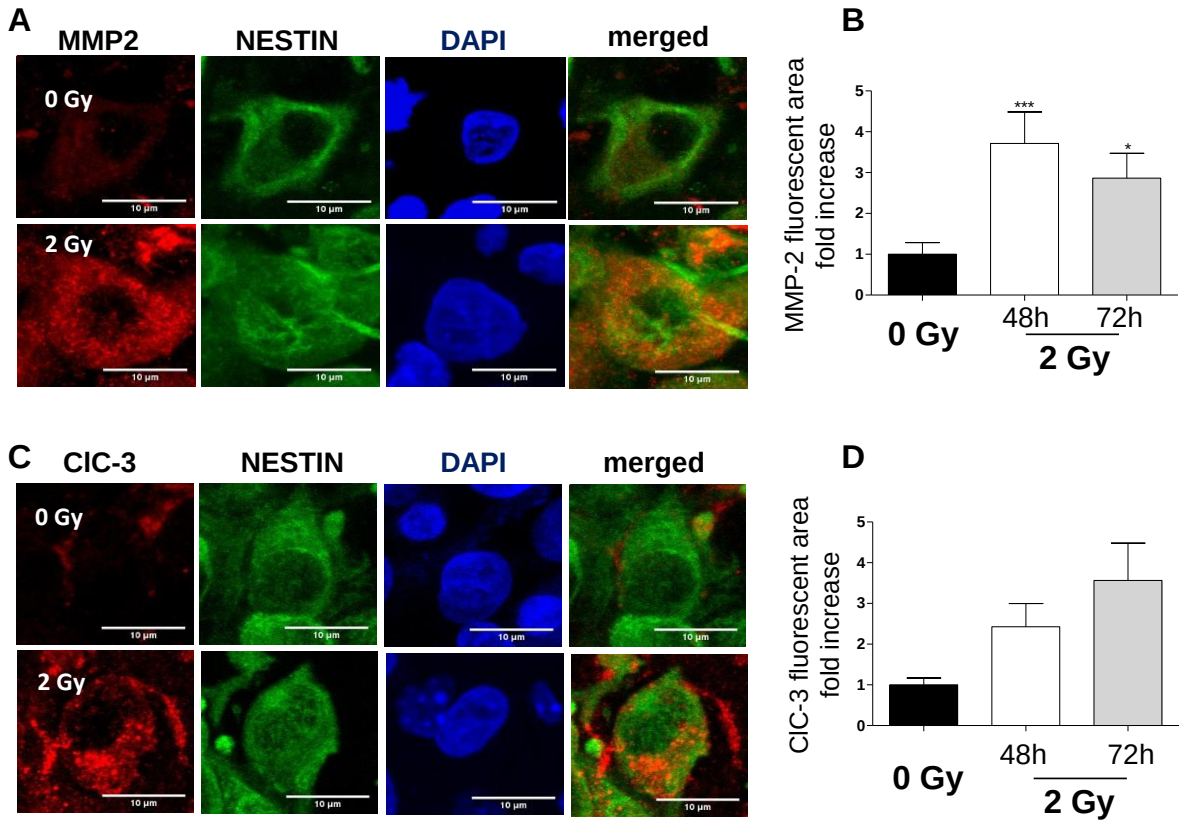

Figure 17. In vivo MMP-2 and ClC3- expression in U87MG xenograft before and after radiations. (A-C) Representative confocal images of brain cryosections from U87MG-trasplanted mice previously irradiated (2Gy) or non-irradiated (0 Gy) and immunostained for human MMP-2 or ClC-3 (red) and nestin (green). Nuclei were revealed by DAPI staining (blue). (B-D) In vivo MMP-2 and ClC-3 level of expression quantification in U87MG xenographs 48 and 72 hours after x-rays treatment. Results are expressed as increased mean MMP-2 and/or ClC-3 fluorescent area respect to non-irradiated samples (0 Gy) ± ES. About 15 microscopy fields for each experimental condition were randomly acquired and analyzed by ImageJ software. For each single microscopy field analyzed MMP-2 and/or ClC-3 fluorescent area was normalized on nuclei number. MMP-2 significance versus non–irradiated tumor cells * p=0,0119; ***p=0,0005.

4.6 CTX-targeted nanovectors act as inhibitor of MMP-2 enzymatic activity

MMP-2, as pointed out before, is a component involved in ECM degradation, in the progression, invasion, and metastasis of malignant lesions [179]. Notably, increase of metastatic tumor activity has been described as a consequence of RT, which

enhances pro-MMP-2 expression [177]. Therefore, whether the binding of CTX-nanovectors to MMP-2 could interfere with its catalytic activity was investigated.

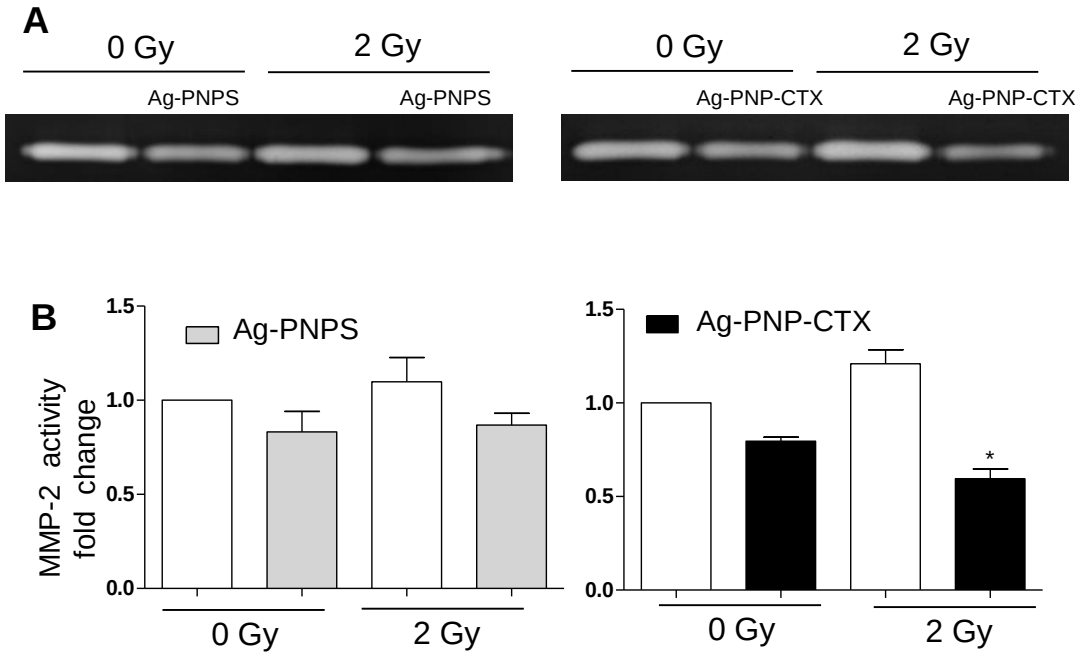

Figure 18. Inhibition of MMP-2 catalytic activity in U87MG cells induced by Ag-PNP-CTX nanovectors. U87MG cells previously irradiated (2Gy) were incubated in the presence of Ag-PNP or Ag-PNP-CTX nanovectors (100 uM for 16 hours). Inhibition of MMP-2 catalytic activity was evaluated by zymography. (A) Representative zymography of one out of 2 independent experiments performed. (B) Densitometry analysis of zimography bands. Results are expressed as mean values from 2 independent experiments normalized to non-irradiated cells (0 Gy) ± ES. Statistical significance was evaluated by One-way ANOVA. Significance versus irradiated cells: *p<0,05.

MMP-2 activity was evaluated by zimography. After a single dose of x rays (2 Gy) U87MG cells were incubated O/N with non-targeted Ag-PNP and targeted Ag-PNP-CTX nanovectors. Remarkably, MMP-2 catalytic activity was inhibited of about 50% exclusively in cells incubated with targeted Ag-PNP-CTX nanovectors while no changes were observed in irradiated cells incubated with non-targeted Ag-PNP nanovectors (Figure 18). Thus, CTX-PNP nanovectors could attain synergistic dual therapeutic effects, tumor-specific intracellular drug-delivery and inhibition of MMP-2 activity.

4.7 In vivo biodistribution of encapsulated Ag-nps

In addition to the Ag-nps accumulation in the brain, Ag-PNP-CTX nanovector biodistribution in peripheral organs was assessed. After Ag-PNP-CTX intra peritoneal injection, animals have been sacrificed at selected time points (24h and 48h after injection) and several tissues including liver, spleen, lung, heart and kidney have been examined in order to quantify the amount of Ag-nps by Inductively Coupled Plasma Mass Spectrometry (ICP-MS). As expected, Ag-PNP-CTX particles have been mostly found in the reticuloendothelial system (RES) organs (liver, ~80%, and spleen, ~ 4% of the injected Ag-nps). Only 2 % of the injected Ag-nps have been found in the lung and a remarkable washout has been observed at 48 hours after nanovector delivery. A very low number of Ag-PNP-CTX nanovectors have been found in the kidney and in the hearth (Figure 19).

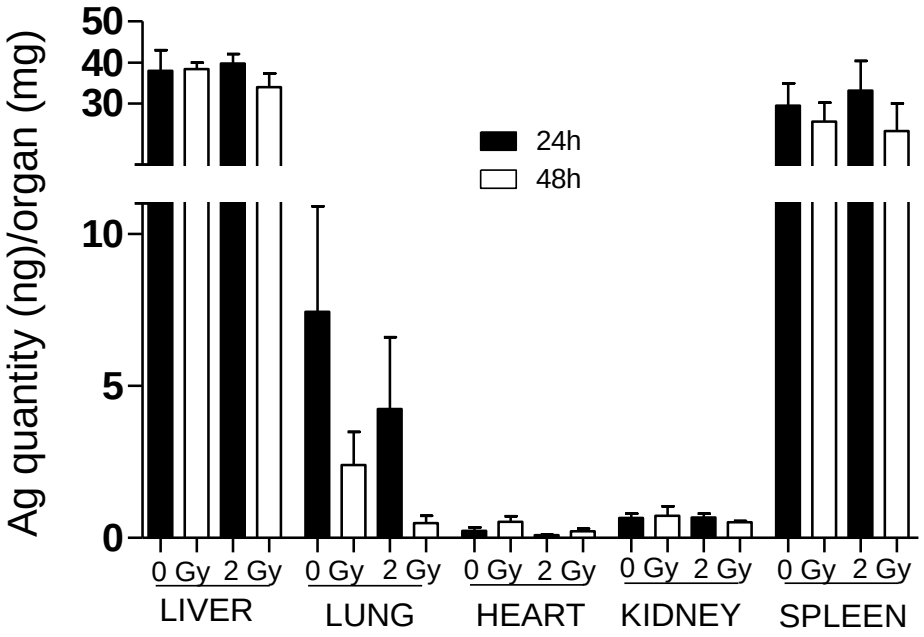

Figure 19. Ag-NP-CTX biodistribution in peripheral organs was evaluated in fresh, non-fixed organs from non-irradiated (0 Gy) and irradiated (2 Gy) U87MG orthotopic transplanted mice (4 mice /experimental group for a total of 16 mice analyzed). Fifteen days after implantation of tumor cells, Ag-PNP-CTX were administered intraperitoneally at a dose of 1mg/mouse. Animals were sacrificed 24 or 48 hours after nanovector injection. Ag-nps quantification was assessed by Inductively Coupled Plasma Mass Spectrometry (ICP-MS) (NEOTRON, Modena, Italy). Results are expressed as amount of Ag detected in 1 mg of the indicated organ ± SE.

4.8 Radiations enhance Ag-PNP-CTX cytotoxic activity against U87MG GBM human cell line

Recently, the possibility of using Ag-nps as antitumoral agents for GBM, either alone [172, 180] or in synergy with other kinds of drugs [172], after entrapment in biocompatible PNPs has been explored.

Thus, a possible synergistic effect of a 2Gy radiation treatment combined with Ag-PNP-CTX administration on U87MG cell growth and viability was investigated.

Irradiated and non-irradiated U87MG cells have been incubated with different Ag-PNP-CTX nanovectors concentration for 72h; thereafter, cell viability has been assessed by MTT test. Other U87MG cells have been treated with either nanovectors without Ag-nps (PNP-CTX), in order to assess polymer and CTX toxicity, or non-targeted nanovectors (Ag-PNP), as a control. As expected, no cellular toxicity has been observed by incubating U87MG cells with empty PNP-CTX nanovectors, while the presence of CTX on the Ag-PNP surface has been found to trigger a dose-dependent inhibition of cell growth induced by the encapsulated Ag-nps. More remarkably, a synergic reduction of U87MG cell viability has been observed when 2 Gy irradiation is delivered before Ag-PNP-CTX incubation. Pro-apoptotic synergic effects have been detected also in vivo in U87MG-transplanted mice. The detection and quantification of apoptotic bodies by in situ terminal deoxynucleotidyl transferase dUTP nick end labeling (TUNEL) assay has shown a significant increase in the amount of apoptotic bodies in irradiated U87MG xenografts and of Ag-PNP-CTX nanovectors vs. U87MG xenografts treated with CTX nanovectors or exposed to radiations as single agents (Figure 20 B). Additional support to the TUNEL results have been provided by bioluminescence imaging (BLI) analysis carried out in luciferase-transfected U87MG (U87MGluc2) xenografts in order to monitor tumor growth over the treatment period (Figure 20 C and D). Eleven days after U87MGluc2 cells implantation (T=0), mice have been divided into 4 groups: untreated mice; mice treated with radiations (2Gy, single dose); mice treated with serial injections of Ag-PNP-CTX single agent (2 doses of 1mg dry matter per mouse, followed by 2 doses of 0,5 mg dry matter per mouse; interval time: 48-72 hours); mice concomitantly treated with radiations and Ag-PNP-CTX.

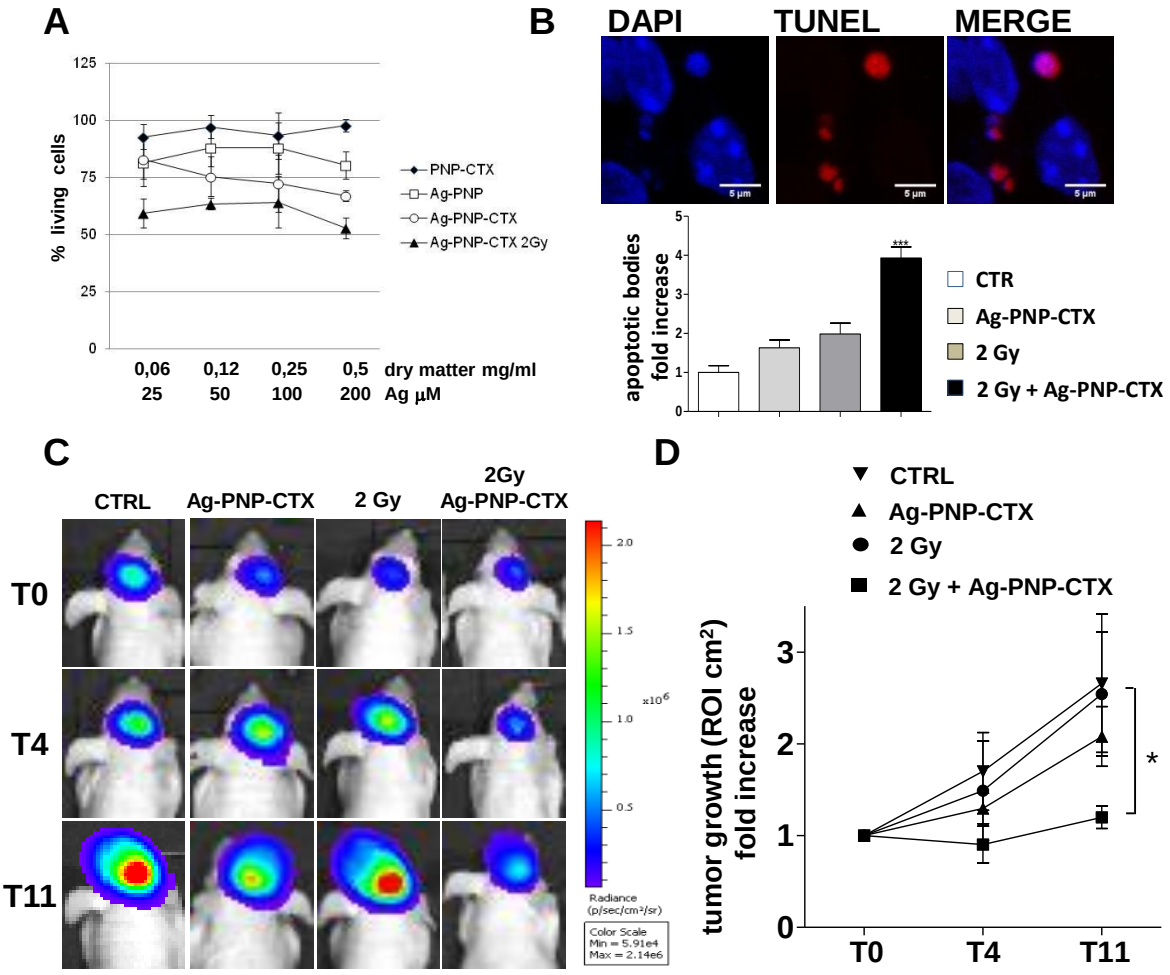

Figure 20. Effect of Ag-nps entrapped into PNP-CTX nanovectors on irradiated (2 Gy) and non-irradiated U87MG cells and tumors viability. (A) Upon treatment with the indicated nanovectors cell survival fraction was measured by MTT assay. Cells were exposed to increasing concentrations of Ag-nps for 72 hours The obtained relative values were normalized to the values from the corresponding untreated cells and are shown as percentage survival. Results are expressed as mean percentage of 3 independent experiments performed in triplicates ± SD. (B) In situ detection of apoptosis by DAPI/TUNEL staining and quantification of apoptotic bodies (1-5 mm size) in U87MG cryosections from non-irradiated and irradiated (2 Gy) mice injected with Ag-PNP-CTX nanovectors. Animals were sacrificed 48 hours after nanovector injection. Four mice/experimental group were analyzed. Results are expressed as mean values normalized to CTR values ± ES. (C) Luciferase imaging of representative mice: untreated (CTRL, 4 mice); injected with Ag-PNP-CTX nanovectors as single agent (2 doses of 1mg/mouse followed by 2 doses of 0,5 mg/mouse, administration interval: 48-72 hours, 5 mice); irradiated (2 Gy single dose, 6 mice); treated with radiations and concomitant Ag-PNP-CTX nanovectors (6 mice). Treatments started 11 days after U87MGluc2 cell implantation (T0=D11). (D) Tumor growth during 11 days of observation measured by area detected setting automatic ROI (50%). Results are expressed as mean values normalized to T0 values ± SE. Statistical significance was evaluated by Paired T test. Significance: *p=0,0177.

As illustrated in Figure 20 C, which shows representative images of single animals from each experimental group, and 20 D, which shows the quantitative analysis of the tumor regions, synergic radiation and CTX-nanovectors treatment has inhibited tumor growth and progression. No inhibitory effect has been observed in mice treated with either radiations or Ag-PNP-CTX only.

5 Discussion

The aim of this work has been to evaluate the efficacy of nanotechnologies for the treatment of GBM. In particular, the capacity of Ag-PNP-CTX nanovectors to target GBM cells has been assessed in vitro and in vivo.

The PLGA-b-PEG core polymer has been chosen for two main reasons. First it has been approved by the Food and Drug Administration (FDA) for human medical usage in view of its good biocompatibility and low toxicity. Indeed, PLGA-b-PEG is already employed in clinical trials [181]. Second reason concerns the distinctive chemical-physical features of this material. One of these features is the versatility of PLGA-b-PEG nanocarriers: they can be loaded with many types of substances such as different drugs and/or cytotoxic molecules including nucleic acids. These nanovectors protect their contents, thus increasing payload half-life, particularly important for the in vivo efficacy. Another advantage is that they do not activate inflammatory responses, such as opsonization [182]. Due to their chemical composition, PLGA-b-PEG allows nanovectors to release its content gradually [183].

In this work the polymeric core (PNP) has been loaded with silver nanoparticles (Ag-nps). Taking advantage of the high contrast provided by Ag-nps they have been used as contrast agents for optical/confocal microscopy detection and imaging of PNPs. In this way, the main advantage is that nanovectors can be visualized without adding fluorescent dyes, thus avoiding chemical modification of the external shell of the nanocarriers, and the subsequent alteration in PNP behavior in the body.
Due to the high stability of Ag-nps and the absence of photobleaching phenomena, Ag-nps represent a very efficient imaging tool for single-cell analysis, characterized by extreme precision and quality with respect to standard fluorescence-based techniques. The light reflection property of Ag-nps allows one to acquire Ag-nps signals with the laser set in reflection mode, without affecting the freedom of choice

of fluorescent markers when the localization of different proteins has to be studied in multicolor experiments. Moreover a fluorescent moiety, linked or adsorbed onto the external surface, may undergo leakage phenomena from the nanosystem once in the body environment, which can lead in turn to unspecific fluorescence detection in not really targeted cells; on the contrary, Ag-nps being strongly entrapped inside the polymeric matrix, are stable and not subjected to this inconvenience. As a general rule, the use of Ag-nps-loaded nanovectors may represent a valuable tool to measure the delivery potential and/or to define the proper administration route and scheduling of drug-loaded nanovectors of interest. Therefore, the use of precise and quantitative methods to track systemically injected nanovectors is of crucial relevance to evaluate and foresee their potential therapeutic efficacy. Indeed, Ag-nps enabled the localization of Ag-PNP-CTX nanovectors in the intracellular compartment (such as the endosomes and lysosomes), and to study in vivo tumor localization at single-cell level.

Another advantage of using PLGA-b-PEG nanovectors concerns the possibility of functionalizing the polymeric surface with peptides able to recognize specific targets. This contributes to significantly increase the amount of uptake, and, in principle, to deliver drug-loaded nanovectors towards the desired target, thus decreasing the side effects with respect to a free drug.

The experiments reported in this work have demonstrated the effectiveness of CTX in increasing Ag-nps uptake in GBM cells in vitro. The competitivity assay has shown that the binding between CTX and the polymeric core nanoparticle does not compromise the possibility of recognition of CTX on its targets, MMP2 and ClC-3 known to be overexpressed in high grade glioma cells [41, 73].
This kind of nanovectors can be functionalized with a wide variety of ligands. In principle, one could even functionalize with more than one ligand at the same time, thus making them selective to different targets and multi-functional. This strategy could improve the effectiveness of the therapeutic strategy, especially in view of the high heterogeneity of GBM cells and the fact that different targets are expressed on the surface of GBM cells differing from one other in the degree of differentiation

[184]. The same nanovectors could then target a wide variety of GBM cells. Due to the fact that its intracellular uptake is receptor-mediated, CTX-nanovectors might be able to bypass the obstacle imposed by multi-drug resistance proteins situated on the cell membrane and that concur to decrease the amount of drug available in the cytoplasm and the efficacy of the drugs.

The CTX-mediated endocytosis of nanovectors is receptor-dependent. In some cases, the vesicles resulting from endocytosis converge in lysosomes [173]. Due to the particular features of the polymer, and especially by virtue of the z-potential being very far from 0, the nanovector can eventually escape from the endo-lysosomal pathway, thus preventing its content from being degraded by the lysosomal enzymes [185,186]. This phenomenon, called endosomal/lysosomal escape can be produced by several mechanisms depending on the chemical nature of the nanovector [187]. One of the mechanisms reported in the literature which might provide the basis to explain the escape of the Ag-PNP-CTX nanovectors is the “proton sponge effect” [188]. the hypothesis is that the presence of the negatively charged nanoparticles (ζ-potential = -30mV) is balanced by the influx of positive charges (H+) into the endosome. This influx of protons causes an influx of Cl- which balances the excess of positive charge. The consequent influx of water, together with the destabilization of the endosome membrane caused by the negative charge of the nanoparticle, breaks the endosome causing release of its content in the cytoplasm.

The presence of the BBB contributes to the current GBM therapeutic constraints by limiting the amount of chemotherapeutics reaching disperse tumor cells infiltrating the brain parenchyma.
Part of this work has been devoted to assess whether nanotechnologies can help to overcome this problem. While the integrity of the BBB would guarantee reduced nanovectors off-target brain toxicity, it makes infiltrating and metastatic GBM cells inaccessible to nanovectors. It is worth noting that CTX, while is able to recognize with high affinity GBM cells, it is not an agent for BBB crossing, thus nanovector brain biodistribution could be limited by the presence of this barrier. As radiotherapy RT is a mainstay of GBM therapy regimens [15, 20] and is known to affect BBB

permeability [189, 190] the effects of radiations on Ag-PNP-CTX tumor accumulation have been assessed.
To mimic to the greatest possible extent one of the current clinical RT protocols used to treat GBM patients (60 Gy delivered in fractions of 2 Gy) [20] we have chosen 2 Gy as a standard experimental RT dosage. As hypothesized, upon radiations a significantly higher quantity of Ag-nps was observed in the tumor area. An increased accumulation was observed at 48 hours from Ag-PNP-CTX injection compared to 24 hours, suggesting an enhanced permeability and retention (EPR) effect, which may prevent nanovectors wash-out and facilitate their accumulation. Interestingly, radiation treatment has been shown not to determine an increased accumulation of Ag-nps in the healthy brain parenchyma.

As expected, in the proximity of the peripheral zone of the tumor we have observed a normal claudin-5 expression, suggestive of an intact BBB. Indeed, no Ag-nps accumulation has been found in the nestin-positive cells found in the tumor periphery and/or far from the tumor mass. However, after 2 Gy radiation treatment – which is known to increase BBB permeability – Ag-nps have been detected in the isolated GBM cells branching into the healthy parenchyma

Differently from healthy brain, the tumorigenic GBM microenvironment promotes neo-angiogenesis and disruption of BBB integrity [191]. The permeabilization of the BBB in the tumor area allows in fact penetration and retention of Ag-nps within the non-irradiated GBM-tumor, although at a lesser extent compared to the irradiated one. Even though low doses of radiations have been shown to be enough to determine in vivo tight junction deregulation (Figure 5B), the presence of a compromised BBB didn’t allow significant accumulation of Ag-nps in irradiated healthy brain parenchyma (Figure 4). This is consistent with the presence, surrounding the brain vessels, of pericytes and astrocytes that contribute to hindering the passive passage of nanovectors [192]. Furthermore, the interstitial fluid pressure and the width of the extracellular space impact on nanovector access and penetration within the healthy parenchyma. It is conceivable that extra-cellular matrix (ECM) components would physically restrict the motion of nanovector in convection through the extracellular

space. It was previously reported that the extracellular spaces in normal brain are between 38 and 64 nm [163]. Therefore, 100nm-sized CTX-nanovectors, likewise the ones used in this study, would hardly diffuse and accumulate in healthy brain tissue.
The lack of Ag-nps accumulation in infiltrating GBM cells in the absence of radiation treatment is compatible with the possibility that, besides favoring permeabilization of the BBB, ionizing radiations, by enhancing the expression of cellular proteases, including MMP-2, play a crucial role in degradation and remodeling of brain ECM thereby facilitating extravasation, convective movements and diffusion of CTX-nanovectors.
This is relevant in the clinical setting, where RT is applied not only to the tumor area but extended to a 2 cm surrounding margins where invading GBM stem-like cells escape to surgery and survive to RT [193,194]. Thus the concomitant use of CTX-nanovectors during RT should facilitate and enhance drug-delivery to the invading and metastatic GBM cells that are the responsible for the majority of the recurrences.

Even though the results obtained in vitro indicated a noteworthy increase of ClC-3 expression compared to MMP-2 after radiation treatment, the in vivo ClC-3 and MMP-2 levels were comparable, suggesting an equivalent contribution for nanovectors cellular uptake and internalization. Indeed the assessment of MMP2 activity in presence of CTX shows that the process of recognizing and internalizing CTX-conjugated nanoparticles leads to a 50% decrease of the proteolic activity, thus suggesting that the use of CTX can have the dual role of directing nanovectors towards the target and of decreasing the side effects related to radiation-induced invasivity. It is reasonable to suppose that CTX conjugated to the polymer can also interfere with ClC-3 activity, by inhibiting the contribution of this channel to cellular motility as it has been already shown in studies on free CTX [76, 195].

As polymeric material is used in some clinical trials [181] we have tried to check whether our system is effective against tumor growth. Moderate toxicity of Ag has been detected, consistently with the literature [172, 180]. The experiments carried out to assess the toxicity of Ag-PNP-CTX in vitro and in vivo have provided a proof-of-

concept of the therapeutic validity of a combination strategy based on radiation therapy and CTX-targeted polymeric nanovectors, which is expected to strengthen the anti-tumor efficacy of any cytotoxic molecules entrapped into PNP-CTX nanovectors.

6 Conclusions

In this work, a nano-technological strategy has been proposed for the management of GBM that addresses two relevant obstacles to effective therapy:
1) the infiltrative nature of GBM;
2) the increase of MMP-2 expression following radiotherapy.
Overall the results showed that (1) although large and advanced GBM tumors disrupt the BBB sufficiently to allow extravasation of functionalized nanocarriers, low dose RT (2 Gy, single dose), by inducing overexpression of proteases such as MMP-2, which also represent CTX molecular targets together with the chloride channel ClC-3, give tumor ECM more porous and permeable to nanovectors, determining their significant enhanced accumulation; (2) differently from the main tumor mass, peripheral GBM tumor niches, where more tumorigenic and invading cells reside, are accessible to engineered nanocarriers exclusively upon radiation treatment; (3) low dose RT is not enough to determine complete BBB disruption preventing nanocarrier accumulation in irradiated healthy brain parenchyma; (4) CTX surface functionalization, besides causing an increased cellular uptake of CTX-targeted nanovectors, inhibits MMP-2 enzymatic activity.

Having demonstrated that an increased nanovectors accumulation and retention can be achieved at significant lower dose of RT (2 Gy), a strong and relevant rationale has been provide for the development of therapeutic strategies able to target tumorigenic and invading GBM cells based on the concomitant administration of RT and CTX-targeted nanovectors. A synergistic therapeutic effect could start from the first fractionated RT dose. Considering that radiations induce the expression of molecules such as MMPs that favor tumor invasion and metastases, the concomitant administration of RT and CTX-targeted nanovectors could represent a significant step forward to GBM management. Indeed, the synergistic effect of CTX-targeted would result from a significant increased accumulation of nanovector therapeutic

cargo inside GBM cells and from the inhibition of approximately 50 % of MMP-2 catalytic activity. These results enable one to conclude that CTX-targeted nanovectors as adjuvants to RT may increase the efficacy of anti-GBM therapies.

7 References

[1] Schiff, D. Quantifying the burden of primary central nervous system malignancy. *Neuro-oncology* . 2015, 287, 1522-8517.

[2] Department of Health and Human Services, Centers for Disease Control and Prevention (CDC), National Program of Cancer Registries (NPCR). Central Brain Tumor Registry of the United States. 2007.

[3] Wrensch, M., Minn, Y., Chew, T., Bondy, M., Berger, M. S. Epidemiology of primary brain tumors: current concepts and review of the literature. *Neuro Oncol*. 2002, 4, 278–299.

[4] Gonzales MF. Classification and pathogenesis of brain tumors. In: Brain Tumors: An Encyclopedic Approach, Churchill Livingstone, Edinburgh 1995. p.31.

[5] Mawrin, C.; Perry, A. Pathological classification and molecular genetics of meningiomas. *J Neurooncol*. 2010, 3, 379-391.

[6] Vignerona, C.; Entz-Werlé, N.; Lutz, P.; Spiegel, A.; Jannier, S.; Helfrec, S.; Alapetitec, C.; Coca, A.; Kehrli, P.; Noël, G. Evolution of the management of paediatric and adult medulloblastoma. *Cancer/Radiothérapie* 2015, 19, 347–357.

[7] Li, K. K. W., Lau, K. M., Ng, H.K. Signaling pathway and molecular subgroups of medulloblastoma. *Int J Clin Exp Pathol*. 2013, 7, 1211–1222.

[8] Goodenberger, ML.; Jenkins, RB. Genetics of adult glioma. *Cancer Genet*. 2012, 12, 613-621.

[9] Korshunov, A.; Meyer, J.; Capper, D.; Christians, A.; Remke, M.; Witt, H.; Pfister, S.; Von Deimling, A.; Hartmann, C.; Combined molecular analysis of BRAF and IDH1 distinguishes pilocytic astrocytoma from diffuse astrocytoma. *Acta Neuropathol*. 2009, 118, 401–405.

[10] Walker, C., Baboire, A., Crooks, D., Wilkins, S., Jenkinson, D. Biology, genetics and imaging of glial cell tumours. *The British Journal of Radiology*. 2011, 84, 90–106.

[11] Louis, D.N., Wiestler, OD., Cavenee, WK. WHO Classification of Tumours of the Central Nervous System. WHO Classification of Tumours of the Central Nervous System. *IARC Press*. 2007,114, 33-49.

[12] Mannucci, P. M., Karimi, M., Mosalaei, A. , Canciani, M. T. , Peyvandi, F. Patients with localized and disseminated tumors have reduced but measurable levels of ADAMTS-13 (von Willebrand factor cleaving protease). *Haematologica*. 2003, 88, 454-458.

[13] Appin, CL., Brat, DJ. Biomarker-driven diagnosis of diffuse gliomas. *Mol. Aspects Med*. 2015, 45, 87-96.

[14] Tatter, SB. Recurrent malignant glioma in adults. Curr. *Treat. Options Oncol*. 2002, 6, 509-524.

[15] Stupp, R., Hegi, M.E., Mason, W.P., Van Den Bent, M.J., Taphoorn, M.J., Janzer, R.C., Ludwin, S.K., Allgeier, A., Fisher, B., Belanger, K., Hau, P., Brandes, A.A., Gijtenbeek, J., Marosi, C., Vecht, C.J., Mokhtari, K., Wesseling, P., Villa, S., Eisenhauer, E., Gorlia, T., Weller, M., Lacombe, D., Cairncross, J.G., Mirimanoff, R.O. Effects of radiotherapy with concomitant and adjuvant temozolomide versus radiotherapy alone on survival in glioblastoma in a randomised phase III study: 5-year analysis of the EORTC-NCIC trial. *Lancet Oncol*. 2009, 5,459-466.

[16] Zhang, X., Zhang, W., Cao, W. D., Cheng, G., Zhang, Y. Q. Glioblastoma multiforme: Molecular characterization and current treatment strategy (Review). *Exp Ther Med*. 2012, 3, 9–14.

[17] Ohgaki, H. and Kleihues, P. The Definition of Primary and Secondary Glioblastoma. *Clin Cancer Res*. 2013, 19; 764-772.

[18] Bastien, J. I.; McNeill, K. A.; Fine, H. A. Molecular characterizations of glioblastoma, targeted therapy, and clinical results to date. Cancer. 2015, 121, 502-516.

[19] Mao, H., Lebrun, D. G., Yang, J., Zhu, V. F., Li, M. Deregulated signaling pathways in glioblastoma multiforme: molecular mechanisms and therapeutic targets. *Cancer Invest*. 2012, 30, 48-56.

[20] Villa, S.; Balana, C.; Comas, S. Radiation and concomitant chemotherapy for patients with glioblastoma multiforme. *Chin J Cancer*. 2014, 33, 25-31.

[21] Maher, E. A., Furnari, F. B., Bachoo, R. M., Rowitch, D. H., Louis, D. N.,. Cavenee, W. K., DePinho, R. A. Malignant glioma: genetics and biology of a grave matter. *Genes & Dev*. 2001, 15, 1311-1333.

[22] Wels, J., Kaplan, R, N.,, Rafii, S., Lyden, D. Migratory neighbors and distant invaders: tumor-associated niche cells. *Genes & Dev*. 2008, 22, 559-574.

[23] Courtneidge, S.A. The 'ins' and 'outs' of podosomes and invadopodia: characteristics, formation and function. *Nature Reviews Molecular Cell Biology*. 2011, 12, 413-426.

[24] Linder, S., Kopp, P. Podosomes at a glance. *Journal of Cell Science*. 2005,118, 2079-2082.

[25] Nakahara, H., Mueller, S.C., Nomizu, M., Yamada, Y., Yeh, Y., Chen, W.T. Activation of beta1 integrin signaling stimulates tyrosine phosphorylation of p190RhoGAP and membrane-protrusive activities at invadopodia. *J Biol Chem*. 1998, 273, 9-12.

[26] Reymond E. Sawaya, R.E., Anderson, M.D., Yamamoto, M. Gokaslan, Z. L., Wu Wang, S., Mohanam, S., Fuller, G.N., McCutcheon, I.E., Stetler-Stevenson, W.G., Nicolson, G.L., Rao, J.S. Expression and localization of 72 kDa type IV collagenase (MMP-2) in human malignant gliomas in vivo. *Clinical & Experimental Metastasis*. 1996, 14, 35-42.

[27] Soroceanu, L., Manning , T. J., Sontheimer, H. Modulation of glioma cell migration and invasion using Cl− and K+ ion channel blockers. *Journal of Neuroscience*. 1999, 19, 5942–5954.

[28] Chang, C., Werb, Z. The many faces of metalloproteases: cell growth, invasion, angiogenesis and metastasis. *Trends Cell Biol*. 2001, 11, 37–43.

[29] Egeblad, M., Werb, Z. New functions for the matrix metalloproteinases in cancer progression. *Nat Rev Cancer*. 2002, 2, 163–176;

[30] John, A., Tuszynsk,i G. The role of matrix metalloproteinases in tumor angiogenesis and tumor metastasis. *Pathology Oncology Research*. 2001, 7, 14–23.

[31] McCawley, L. J., Matrisian, L. M. Matrix metalloproteinases: they’re not just for matrix anymore! *Curr Opin Cell Biol*. 2001, 13, 534–540.

[32] Levicar, N., Nutall, R. K., Lah1, T. T. Proteases in brain tumour progression. *Acta Neurochir (Wien).* 2003, 145, 825-838.

[33] Pagenstecher, A., Stalder, A. K., Kincaid, C. L., Shapiro, S. D., Campbell I. L. Differential expression of matrix metalloproteinase and tissue inhibitor of matrix metalloproteinase genes in the mouse central nervous system in normal and inflammatory states. *Am. J. Pathol*. 1998, 152, 729–741.

[34] Cossins, J. A., Clements, J.M., Ford, J., Miller, K. M., Pigott, R., Vos, W., Van der Valk, P., De Groot, C.J. Enhanced expression of MMP-7 and MMP-9 in demyelinating multiple sclerosis lesions. *Acta Neuropathol*. 1997, 94, 6, 590-598.

[35] Egeblad, M., Werb, Z. New functions for the matrix metalloproteinases in cancer progression. Nat Rev Cancer. 2002, 2, 161-174.

[36] Rundhaug, J. E. Matrix Metalloproteinases, Angiogenesis, and Cancer Commentary re: A. C. Lockhart et al., Reduction of Wound Angiogenesis in Patients Treated with BMS-275291, a Broad Spectrum Matrix Metalloproteinase Inhibitor. *Clin. Cancer Res*. 2003, 9, 551-554.

[37] Reunanen, N., Kähäri, N. Matrix Metalloproteinases in Cancer Cell Invasion . *Landes Bioscience*; 2000. Madame Curie Bioscience Database [Internet].

[38] Nagase, H. Activation mechanisms of matrix metalloproteinases. *Biol. Chem*. 1997,378, 151–160.

[39] Sternlicht, M.D., Werb, Z. How matrix metalloproteinases regulate cell behavior. *Annu Rev Cell Dev Biol*. 2001, 17, 463-516.

[40] Uhm, J. H., Dooley, N. P., Villemure, J. G., Yong, V. W. Glioma invasion in vitro: regulation by matrix metalloprotease-2 and protein kinase C. *Clin. Exp. Metastasis*. 1996, 14, 421–433.

[41] Lampert, K., Machein, U., Machein, M.R., Conca, W., Peter, H. H., Volk, B. Expression of matrix metalloproteinases and their tissue inhibitors in human brain tumors. *Am. J. Pathol*. 1998, 153, 429-37.

[42] Mitra, A., Chakrabarti, J., Banerji, A., Das, S., Chatterjee, A. Culture of human cervical cancer cells, SiHa, in the presence of fibronectin activates MMP-2. *Journal of cancer research and clinical oncology*. 2002, 132, 505–513.

[43] Stanton, H., Gavrilovic, J., Atkinson, S. J., d'Ortho, M. P., Yamada, K. M., The activation of ProMMP-2 (gelatinase A) by HT1080 fibrosarcoma cells is promoted by culture on a fibronectin substrate and is concomitant with an increase in processing of MT1-MMP (MMP-14) to a 45 kDa form. *Journal of cell science*. 1998, 111, 2789–2798.

[44] Moroz, A., Delella, F. K., Lacorte, L. M., Deffune, E., Felisbino, S. L. Fibronectin induces MMP2 expression in human prostate cancer cells. *Biochemical and biophysical research communications*. 2013, 430, 1319–1321.

[45] Das, S., Banerji, A., Frei, E., Chatterjee, A. Rapid expression and activation of MMP-2 and MMP-9 upon exposure of human breast cancer cells (MCF-7) to fibronectin in serum free medium. *Life sciences*. 2008, 82, 467–476.

[46] Brat, D.J., Bellail, A.C., Van Meir, E. G. The role of interleukin-8 and its receptors in gliomagenesis and tumoral angiogenesis. *Neuro Oncol*. 2005, 7, 122–133.

[47] Chernov, A.V., Sounni, N. E., Remacle, A. G., Strongin, A. Y. Epigenetic control of the invasion-promoting MT1-MMP/MMP-2/TIMP-2 axis in cancer cells. *The Journal of biological chemistry*. 2009, 284, 12727–12734.

[48] Chik, F., Szyf, M. Effects of specific DNMT gene depletion on cancer cell transformation and breast cancer cell invasion; toward selective DNMT inhibitors. *Carcinogenesis*. 2011, 32, 224–232.

[49] Festugatto Navarini, N., Cavalcanti de Araújo, V., Brown, A. L., Passador-Santos, F., Fernandes de Souza, I., Napimoga, M. H. Araújo, N. S., Ferreira Martinez, E. The EGF signaling pathway influences cell migration and the secretion of metalloproteinases by myoepithelial cells in pleomorphic adenoma. *Tumor Biology*. 2015, 36, 205-211

[50] Murphy, G., Willenbrock, F., Crabbe, T., O'Shea, M., Ward, R., Atkinson, S., O'Connell, J., Docherty, A. Regulation of matrix metalloproteinase activity. *Ann. N. Y. Acad. Sci*. 1994, 732, 31-41.

[51] Sariahmetoglu, M., Crawford, B. D., Leon, H., Sawicka, J., Li, L.,. Ballermann, B. J., Holmes, C., Berthiaumell, L. G., Holt, A., Sawicki, G., Schulz, R. Regulation of matrix metalloproteinase-2 (MMP-2) activity by phosphorylation. *The FASEB Journal*. 2007, 21, 2486-2495.

[52] Sariahmetoglu, M., Skrzypiec-Spring, M., Youssef, N., Jacob-Ferreira, A. L., Sawicka, J., Holmes, C., Sawicki, G., Schulz, R. Phosphorylation status of matrix metalloproteinase 2 in myocardial ischaemia-reperfusion injury. *Heart*. 2012, 98, 656-662.

[53] Shimokawa, K., Nagase H., Purification of MMPs and TIMPs. *Methods Mol Biol*. 2001;151, 275-304.

[54] Cledennin, N. J., Appelt, K. (eds), *Matrix Metalloproteinase Inhibitors in Cancer Therapy*. Totawa, NJ: Humana Press Inc., 2000.

[55] Itoh, Y., Ito, A., Iwatall, K., Tanzawa, K., Mori, Y., Nagase, H. Plasma Membrane-bound Tissue Inhibitor of Metalloproteinases (TIMP)-2 Specifically Inhibits Matrix Metalloproteinase 2 (Gelatinase A) Activated on the Cell Surface. *The Journal of Biological Chemistry*. 1998, 273, 24360–24367.

[56] Murphy, G., Knauper, V. Relating matrix metalloproteinase structure to function: why the 'hemopexin' domain? *Matrix Biol*. 1997,15, 511–518.

[57] Lu, K. V., Jong, K. A., Rajasekaran, A. K., Cloughesy, T. F., Mischel, P. S. Upregulation of tissue inhibitor of metalloproteinases (TIMP)-2 promotes matrix metalloproteinase (MMP)-2 activation and cell invasion in a human glioblastoma cell line. *Laboratory Investigation*. 2004, 84, 8–20.

[58] Nagase, H., Enghild, J.J., Suzuki, K., Salvesen, G. Stepwise activation mechanisms of the precursor of matrix metalloproteinase 3 (stromelysin) by proteinases and (4-aminophenyl)mercuric acetate. *Biochemistry*. 1990, 29, 5783–5789.

[59] Polette, M., Nawrocki-Raby, B., Gilles, C., Clavel, C., Birembaut, P. Tumour invasion and matrix metalloproteinases. *Crit Rev Oncol Hematol*. 2004, 49, 179-86.

[60] Aimes, R.T., Quigley, J.P. Matrix metalloproteinase-2 is an interstitial collagenase. Inhibitor-free enzyme catalyzes the cleavage of collagen fibrils and soluble native type I collagen generating the specific 3/4- and 1/4-length fragments. *J Biol Chem*. 1995, 270, 5872–5876.

[61] Jentsch, T. J. . Chloride and the endosomal-lysosomal pathway: emerging roles of CLC chloride transporters. *J Physiol*. 2007, 578, 633-640.

[62] Ludewig, U., Pusch, M., Jentsch, T. J. Two physically distinct pores in the dimeric ClC-0 chloride channel. *Nature*. 1996, 383, 340-343.

[63] Jentsch, T. J., Günther, W. Chloride channels: an emerging molecular picture. *Bioessays*. 1997, 19, 117-26.

[64] Blackiston, D. J., McLaughlin, K. A., Levin, M. Bioelectric controls of cell proliferation: ion channels, membrane voltage and the cell cycle. Cell Cycle. 2009, 8, 3519–3528.

[65] Weaver, A.K., Liu, X., Sontheimer, H. Role for calcium-activated potassium channels (BK) in growth control of human malignant glioma cells. *Journal of Neuroscience Research*. 2004, 78, 224–234.

[66] Basrai, D., Kraft, R., Bollensdorff, C., Liebmann, L., Benndorf, K., Patt, S. BK channel blockers inhibit potassium-induced proliferation of human astrocytoma cells. *NeuroReport*. 2002, 13, 403–407.

[67] Salazar, G., Love, R., Styers, M. L., Werner, E., Peden, A., Rodriguez, S., Gearing, M., Wainer, B. H., Faundez, V. AP-3-dependent Mechanisms Control the Targeting of a Chloride Channel (ClC-3) in Neuronal and Non-neuronal Cells. *The Journal of Biological Chemistry*. 2009, 279, 25430-25439

[68] Stobrawa, S. M., Breiderhoff, T., Takamori, S., Engel, D., Schweizer, M., Zdebik, A. A., Bösl, M. R., Ruether, K., Jahn, H., Draguhn, A., Jahn, R., Jentsch, T. J. Disruption of ClC-3, a chloride channel expressed on synaptic vesicles, leads to a loss of the hippocampus. *Neuron*. 2001, 29, 185-196.

[69] Li, X., Wang, T., Zhao, Z., Weinman, S. A. The ClC-3 chloride channel promotes acidification of lysosomes in CHO-K1 and Huh-7 cells. *Am J Physiol Cell Physiol*. 2002, 282, 1483–1491.

[70] Lasse`Gue, B., How Does the Chloride/Proton Antiporter ClC-3 Control NADPH Oxidase? *Circulation Research*. 2007, 101, 648-650.

[71] Verkhratsky, A., Steinhäuser, C. Ion channels in glial cells. *Brain Research Reviews*. 2000, 32, 380–412.

[72] Cuddapah, V. A., Sontheimer, H. Molecular interaction and functional regulation of ClC-3 by Ca2+/calmodulin-dependent protein kinase II (CaMKII) in human malignant glioma. *Journal of Biological Chemistry*. 2010, 285, 11188–11196.

[73] Olsen, M. L., Schade, S., Lyons, S. A., Amaral, M. D., Sontheimer, H. Expression of voltage-gated chloride channels in human glioma cells. *J Neurosci*. 2003, 23, 5572-5582.

[74] McFerrin, M. B., Sontheimer, H. A role for ion channels in glioma cell invasion. *Neuron Glia Biol*. 2006, 2, 39-49.

[75] Cuddapah, V. N., Robel, S., Watkins, S., Sontheimer, H. A neurocentric perspective on glioma invasion. *Nature Reviews Neuroscience*. 2014, 15, 455–465.

[76] Deshane, J., Garner, C. C., Sontheimer, H. Chlorotoxin inhibits glioma cell invasion via matrix metalloproteinase-2. *J Biol Chem*. 2003, 278, 4135-4414.

[77] Stupp, R., Mason, W. P., Man Den Bent, M. J., Weller, M., Fisher, B.,. Taphoorn, M.J. B., Belanger, K.,. Brandes, A.A., Marosi, C., Bogdahn, U., Curschmann, J., Janzer, R.C., Ludwin, S.K., Gorlia, T., Allgeier, A., Lacombe, D., Cairncross, J.G., Eisenhauer, E.,. Mirimanoff, R.O. Radiotherapy plus Concomitant and Adjuvant Temozolomide for Glioblastoma. *N Engl J Med*. 2005, 352, 987-996.

[78] Yan, H., Pearsons, D.W., Jin, G., IDH1 and IDH2 Mutations in Gliomas. *NewEngland Journal of Medicine*. 2009, 360, 765-73.

[79] Stupp, R., Hegi, M. E., Mason, W. P., Van den Bent, M. J., Taphoorn, M. J., Janzer, R. C., Ludwin, S. K., Allgeier, A., Fisher, B., Belanger, K., Hau, P., Brandes, A. A., Gijtenbeek, J., Marosi, C., Vecht, C. J., Mokhtari, K., Wesseling, P., Villa, S., Eisenhauer, E., Gorlia, T.,

Weller, M., Lacombe, D., Cairncross, J. G., Mirimanoff, R. O. Effects of radiotherapy with concomitant andadjuvant temozolomide versus radiotherapy alone on survival in glioblastoma in arandomised phase III study: 5-year analysis of the EORTC-NCIC trial. *Lancet Oncol*. 2009,10, 459-566.

[80] Chan, M. D., Rogers, C. L., Anderson, B., Khuntia, D. Chapter 28 – Benign Brain Tumors: Meningiomas and Vestibular Schwannomas. *Clinical Radiation Oncology (Fourth Edition*). 2016, 483–501.

[81] Silbergeld, D. L.,. Rostomily, R. C.,. Alvord Jr. E. C., The cause of death in patients with glioblastoma is multifactorial: Clinical factors and autopsy findings in 117 cases of supratentorial glioblastoma in adults. *Journal of Neuro-Oncology.* 1991, 10, 179-185.

[82] Kuhnt, D., Becker, A., Ganslandt, O., Bauer, M., Buchfelder, M., Nimsky, C., Correlation of the extent of tumor volume resection and patient survival in surgery of glioblastoma multiforme with high-field intraoperative MRI guidance. *Neuro Oncol*. 2011,13, 1339–1348.

[83] Barani, J. I., Larson, D. A. Radiation Therapy of Glioblastoma. 2014, 163, 49-73.

[84] Qin, DX., Zheng, R., Tang, J., Li, J. X., Hu, Y. H. Influence of radiation on the blood-brain barrier and optimum time of chemotherapy. *Int. J. Radiat. Oncol. Biol. Phys*. 1990, 19, 1507-1510.

[85] Van Vulpen, M., Kal, H. B., Taphoorn, M. J., El-Sharouni, S.Y. Changes in blood-brain barrier permeability induced by radiotherapy: implications for timing of chemotherapy? *Oncol. Rep.* 2002, 9, 683-688.

[86] Beauchesne, P., Bernier, V., Carnin, C., Taillandier, L., Djabri, M., Martin, L., Michel, X., Maire, J. P., Khalil, T., Kerr, C., Gorlia, T., Stupp, R., Pedeux, R. Prolonged survival for patients with newly diagnosed, inoperable glioblastoma with 3-times daily ultrafractionated radiation therapy. *Neuro Oncol*. 2010, 12, 595-602.

[87] Shaw, E., Scott, C., Souhami, L., Dinapoli, R., Kline, R., Loeffler, J., Farnan, N. Single dose radiosurgical treatment of recurrent previously irradiated primary brain tumors and brain metastases: final report of RTOG protocol 90-05. *International Journal of Radiation Oncology-Biology-Physics*. 2000, 47, 291–298.

[88] Sneed, P.K., Lamborn, K.R., Forstner, J.m., McDermott, M.W., Chang, S., Park, E., Gutin, P.H., Phillips, T.L., Wara, W.M., Larson, D.A. Radiosurgery for brain metastases: is whole brain radiotherapy necessary? *International Journal of Radiation Oncology-Biology-Physics.* 1999, 43, 549–558.

[89] Al-Omair, A., Soliman, H., Xu, W., Karotki, A., Mainprize, T., Phan, N., Das, S., Keith, J., Yeung, R., Perry, J., Tsao, M., Sahgal, A. Hypofractionated stereotactic radiotherapy in five daily fractions for post-operative surgical cavities in brain metastases patients with and without prior whole brain radiation. *Technol Cancer Res Treat*. 2013, 12, 493-99.

[90] Scott, J., Tsai, Y. Y., Chinnaiyan, P., Yu, H. H. Effectiveness of radiotherapy for elderly patients with glioblastoma. *Int J Radiat Oncol Biol Phys*. 2011, 81, 206-10.

[91] Stewart, L.A. Chemotherapy in adult high-grade glioma: a systematic review and meta-analysis of individual patient data from 12 randomised trials. *The Lancet*. 359, 9311, 1011–1018.

[92] Shaw, E., Arusell, R., Scheithauer, B., O'Fallon, J., O'Neill, B., Dinapoli, R., Nelson, D., Earle, J.,. Jones, C., Cascino, T., Nichols, D., Ivnik, R., Hellman, R., Curran W.,. Abrams, R. Prospective Randomized Trial of Low- Versus High-Dose Radiation Therapy in Adults With Supratentorial Low-Grade Glioma: Initial Report of a North Central Cancer Treatment. *J Clin Oncol*. 2002, 20, 2267-2276.

[93] Spostol, R., Ertel, I. J., Jenkin, R. D. T., Boesel, C. P., Venes, J. L.,. Ortega, J. A., Evans, A. E., Waral, W., Hammond, D. The effectiveness of chemotherapy for treatment of high grade astrocytoma in children: Results of a randomized trial. *Journal of Neuro-Oncology*. 1989, 7, 165-177.

[94] Glenn, M. D., Sheline, E. Radiotherapy for high grade gliomas. *International Journal of Radiation Oncology*Biology*Physics*. 18, 4, 793-803.

[95] Park, C. M.; Park, M. J.; Kwak, H. J.; Lee, H. C.; Kim, M. S.; Lee, S. H.; Park, I. C.; Rhee, C. H.; Hong, S. I. Ionizing radiation enhances matrix metalloproteinase-2 secretion and invasion of glioma cells through Src/epidermal growth factor receptor-mediated p38/Akt and phosphatidylinositol 3-kinase/Akt signaling pathways. Cancer Res. 2006, 66, 8511-8519.

[96] Wild-Bode, C., Weller, M., Rimner, A., Dichgans, J., Wick, W. Sublethal irradiation promotes migration and invasiveness of glioma cells: implications for radiotherapy of human glioblastoma. *Cancer Res*. 2001, 61, 2744-50.

[97] Qian, L. W., Mizumoto, K., Urashima, T., Nagai, E., Maehara, N., Sato, N., Nakajima, M., Tanaka, M. Radiation-induced increase in invasive potential of human pancreatic cancer cells and its blockade by a matrix metalloproteinase inhibitor, CGS27023. *Clin Cancer Res*. 2002,8, 1223-1227.

[98] Camphausen, K., Moses, M. A., Beeken, W. D., Khan, M. K., Folkman, J., O' Reilly, M.S. Radiation therapy to a primary tumor accelerates mestastatic growth in mice. 2001, 61, 2207-2211.

[99] Wick, W., Platten, M., Weller, M. New (alternative) temozolomide regimens for the treatment of glioma. *Neuro Oncol*. 2009, 11, 69-79.

[100] Minniti, G., Muni, R., Lanzetta, G., Marchetti, P., Enrici, R. M. Chemotherapy for glioblastoma: current treatment and future perspectives for cytotoxic and targeted agents. *Anticancer Res*. 2009, 29, 5171-5184.

[101] Crespo, I., Vital, A. L., Gonzalez-Tablas†, M., del Carmen Patino, M., Otero, A., Lopes, M. L., , de Oliveira, C., Domingues, P., Orfao, A., Tabernero, M. D. , Molecular and Genomic Alterations in Glioblastoma Multiforme. *The American Journal of Pathology.* 185, 7, 1820–1833.

[102] Becker, I., Becker, K. F., Meyermann, R., Höllt, V. The multidrug-resistance gene MDR1 is expressed in human glial tumors. *Acta Neuropathol*. 1991, 82, 516-519.

[103] Borst, P., Evers, R., Kool, M., Wijnholds, J. The multidrug resistance protein family. *Biochim Biophys Acta*. 1999, 1461, 347-357.

[104] Cordes, N, Seidler, J., Durzok, R., Geinitz, H., Brakebusch, C. Beta1-integrin-mediated signaling essentially contributes to cell survival after radiation-induced genotoxic injury. *Oncogene*. 2006, 25, 1378–1390.

[105] Monferran, S., Skuli, N., Delmas, C., Favre, G., Bonnet, J., Cohen-Jonathan-Moyal, E., Toulas, C. avb3 and avb5 integrins control glioma cell response to ionizing radiation through ILK and RhoB. *Int. J. Cancer*. 2008, 123, 357–364.

[106] Kumar, C. C. Integrin alpha v beta 3 as a therapeutic target for blocking tumor-induced angiogenesis. *Curr Drug Targets*. 2003, 4, 123-131.

[107] Altaner, C. Glioblastoma and stem cells. *Neoplasma*. 2008, 55, 369-374.

[108] Ropolo, M., Daga, A., Griffero, F., Foresta, M., Casartelli, G., Zunino, A., Poggi, A., Cappelli, E., Zona, G., Spaziante, R., Corte, G., Frosina, G. Comparative analysis of DNA repair in stem and nonstem glioma cell cultures. *Mol Cancer Res*. 2009, 7, 383-392.

[109] Shi, L., Chen, J., Yang, J., Pan, T., Zhang, S., Wang, Z. MiR-21 protected human glioblastoma U87MG cells from chemotherapeutic drug temozolomide induced apoptosis by decreasing Bax/Bcl-2 ratio and caspase-3 activity. *Brain Res*. 2010, 1325, 255-264.

[110] Bao, S., Wu, Q.,. McLendon, R. E., Hao, Y., Shi,Q., Hjelmeland, a. b., Dewhirst, M. W., Bigner; D. D., Rich, J. N. Glioma stem cells promote radioresistance by preferential activation of the DNA damage response. *Nature*. 2006, 444, 756-760.

[111] Charles, N. A., Holland, E. C. , Gilbertson, R., Glass, R., Kettenmann, H. The brain tumor microenvironment. *Glia*. 2011, 59, 1169-1180.

[112] Oliver, L., Olivier, C., Marhuenda, F. B., Campone, M., Vallette, F. M. Hypoxia and the malignant glioma microenvironment: regulation and implications for therapy. *Curr. Mol. Pharmacol*. 2009, 2, 263-284.

[113] Li, Z., Bao, S., Wu, Q., Wang, H., Eyler, C., Sathornsumetee, S., Shi, Q., Cao, Y., Lathia, J., McLendon, R. E., Hjelmeland, A. B., Rich, J. N. Hypoxia-inducible factors regulate tumorigenic capacity of glioma stem cells. *Cancer Cell*. 2009, 15, 501-513.

[114] Sarkaria, J. N., Kitange,G. J., James,C. D., Plummer, R., Calvert, H., Weller, M., Wick, W. Mechanisms of Chemoresistance to Alkylating Agents in Malignant Glioma. *Clin. Cancer. Res.* 2008; 14.

[115] Sarkaria, N., Kitange,2 C. David James,1 Ruth Plummer,3 Hilary Calvert,3 Michael Weller,4 and Wolfgang Wick4. Mechanisms of Chemoresistance in Malignant Glioma. *Clin Cancer Res*. 2008 May 15; 14(10): 2900–2908.

[116] Azria, D., Larbouret, C., Robert, B., Culine, S., Ychou, M., Verrelle, P., Dubois, J.B., Pèlegrin, A. Radiotherapy and inhibitors of epidermal growth factor receptor: preclinical findings and preliminary clinical trials*. Bull Cancer*. 2003, 90, 202-212.

[117] Hovinga, K. E. , Stalpers, L. J. , van Bree, C., Donker, M., Verhoeff, J. J. , Rodermond, H. M., Bosch, D. A. , van Furth W. R. Radiation-enhanced vascular endothelial growth factor (VEGF) secretion in glioblastoma multiforme cell lines:a clue to radioresistance? *J Neurooncol.* 2005, 74, 99-103.

[118] Kreuter, J. Drug delivery to the central nervous system by polymeric nanoparticles: what do we know? *Adv Drug Deliv Rev*. 2014, 71, 2-14.

[119] Agarwal, S., Manchanda, P., Vogelbaum, M. A., Ohlfest, J. R., Elmquist, W. F. Function of the blood-brain barrier and restriction of drug delivery to invasive glioma cells: findings in an orthotopic rat xenograft model of glioma. *Drug Metab Dispos*. 2013, 41, 33-39.

[120] Woodworth, G. F., Dunn, G. P., Nance, E. A., Hanes, J., Brem, H. Emerging insights into barriers to effective brain tumor therapeutics. *Front Oncol*. 2014, 4, 126,

[121] Lim, J.C., Kania, K.D., Wijesuriya, H., Chawla, S., Sethi, J.K., Pulaski, L., Romero, I.A., Couraud, P.O., Weksler, B.B., Hladky, S.B., Barrand, M.A. Activation of β-catenin signalling by GSK-3 inhibition increases p-glycoprotein expression in brain endothelial cells. *J. Neurochem*. 2008, 106, 1855–1865.

[122] Choi, Y.K., Kim, K.W.,. Blood–neural barrier: its diversity and coordinated cell-to-cell communication. *BMB*. 2008, 41, 345–352.

[123] Abbott N., Rönnbäck, L., Hansson, E. Astrocyte-endothelial interactions at the blood-brain barrier. *Nat Rev Neurosci*. 2006, 7, 41-53.

[124] Ballabh, P. , Braun. A., Nedergaard, M. The blood–brain barrier: an overview: Structure, regulation, and clinical implications. *Neurobiology of Disease.* 2004,1, 1-13.

[125] Hawkins, R. A., O'Kane, R. l., Simpson, I. A., Viña, J. R.. Structure of the Blood–Brain Barrier and Its Role in the Transport of Amino Acids1–3. J. *Nutr*. 2006, 136, 218-226.

[126] Chaudhuri J. D. Blood brain barrier and infection. *Med Sci Monit*. 2000, 6, 1213-1222.

[127] de Boer, A. G., Gaillard, P. J. Blood-brain barrier dysfunction and recovery. *J Neural Transm.* 2006, 113, 455-62.

[128] Abbott, N. J. Astrocyte-endothelial interactions and blood-brain barrier permeability. *J Anat*. 2002, 200, 629-38.

[129] Zheng, W., Aschner, M., Ghersi-Egeac, J. F. Brain barrier systems: a new frontier in metal neurotoxicological research. *Toxicol Appl Pharmacol*. 2003, 192, 1–11.

[130] Yamagata, K., Matsumura, K., Inoue, W., Shiraki, T., Suzuki, K., Yasuda, S., Sugiura, H., Cao, C., Watanabe, Y., Kobayashi, S. Coexpression of Microsomal-Type Prostaglandin E Synthase with Cyclooxygenase-2 in Brain Endothelial Cells of Rats during Endotoxin-Induced Fever. *The Journal of Neuroscience*. 2001, 21, 2669-2677;

[131] Barber, A. J., Lieth, E. Agrin accumulates in the brain microvascular basal lamina during development of the blood-brain barrier. *Developmental Dynamics*. 1997; 208, 62-74.

[132] Carvey, P. M., Hendey, B., Monahan, A. J.. The Blood Brain Barrier in Neurodegenerative Disease: A Rhetorical Perspective. *J Neurochem*. 2009, 111, 291–314.

[132] Timpl, R.,. Brown, J. C. The laminins. *Matrix Biology* 1994, 14, 275–28.

[133] Timpl, R., Rohde, H., Robey, P. G., Rennard, S. I., Foidart, J. M., Martin, G. R. Laminin--a glycoprotein from basement membranes. *J Biol Chem*. 1979, 254, 9933-9937.

[134] Takahashi, K., Nakata, Y., Someya, K., Hattori, M. Improvement of the Physical Properties of Pepsin-Solubilized Elastin-Collagen Film by Crosslinking. *Biosci Biotechnol Biochem*. 1999, 63, 2144-2149.

[135] Abbott, N. J., Patabendige, A. A.K., Dolman, D. E. M., Yusof, S. R.,. Begley, D. J. Structure and function of the blood–brain barrier. *Neurobiology of Disease*. 2010, 37, 13–25.

[136] Kaur, C., Ling, E. A. Blood brain barrier in hypoxic-ischemic conditions. *Curr Neurovasc Res*. 2008, 5, 71-81.

[137] Wolburg, H., Lippoldt, A. Tight junctions of the blood-brain barrier: development, composition and regulation. *Vascul Pharmacol*. 2002, 38, 323-37.

[138] Begley, D. J., Brightman, M. W. Structural and functional aspects of the blood-brain barrier. *Prog Drug Res*. 2003, 61, 39-78.

[139] Khasraw, M., Ameratunga, M. S., Grant, R., Wheeler, H., Pavlakis, N. Antiangiogenic therapy for high-grade glioma. *Cochrane Database Syst Rev*. 2014, 9, 1361-6137.

[140] Wolburg, H., Noellb, S., Fallier-Beckera, P.,. Mackc, A. F., Wolburg-Buchholza, K. The disturbed blood–brain barrier in human glioblastoma. *Molecular Aspects of Medicine.* 2012, 33, 579-589.

[141] Noël,A., Gutiérrez-Fernández, A., Sounni, E., Behrendt, N., Maquoi, E., Lund, I. K., Santiago Cal,2 Gunilla Hoyer-Hansen,3,4 and Carlos López-Otín2. New and Paradoxical Roles of Matrix Metalloproteinases in the Tumor Microenvironment. Front Pharmacol. 2012; 3: 140. Published online 2012 Jul 17.

[142] Rascher, G., Fischmann, A., Kröger, S., Duffner, F., Grote, E. H., Wolburg, H. Extracellular matrix and the blood-brain barrier in glioblastoma multiforme: spatial segregation of tenascin and agrin. *Acta Neuropathologica*. 2002, 104, 85-91.

[143] Liebner, S., Fischmann, A., Rascher, G., Duffner, F., Grote, E.-H., Kalbacher, H., Wolburg, H. Claudin-1 and claudin-5 expression and tight junction morphology are altered in blood vessels of human glioblastoma multiforme. *Acta Neuropathologica*. 2000, 100, 323-331.

[144] Carvey,P. M., Hendey,B., Monahan, A. J. The Blood Brain Barrier in Neurodegenerative Disease: A Rhetorical Perspective. *J Neurochem*. 2009, 111, 291–314.

[145] Trnovec, T., Kállay, Z., Bezek, Š. Effects of ionizing radiation on the blood brain barrier permeability to pharmacologically active substances. *International journal of radiation oncology, biology, physics*. 1990, 19, 1581–1587.

[146] Sándor,N., Walter, F. R., Bocsik, A., Sántha, P., Schilling-Tóth,B., Léner, V., Varga, Z., Kahán, Z., Deli, A. M., Sáfrány, G., Hegyesi, H. Low Dose Cranial Irradiation-Induced Cerebrovascular Damage Is Reversible in Mice. *PLoS One*. 2014, 9, e112397.

[147] Wohlfart, S., Gelperina, S., Kreuter, J. Transport of drugs across the blood-brain barrier by nanoparticles. J Control Release. 2012, 161, 264-273.

[148] Kievit, F. M., Zhang, M. Cancer nanotheranostics: improving imaging and therapy by targeted delivery across biological barriers. *Adv Mater*. 2011, 23, 217-247.

[149] Hobbs, S. K., Monsky, W. L., Yuan, F.; Roberts, W. G., Griffith, L.; Torchilin, V. P., Jain, R. K. Regulation of transport pathways in tumor vessels: role of tumor type and microenvironment. Proc Natl Acad Sci U.S.A. 1998, 95, 4607-4612.

[150] Gao, H., Yang, Z., Zhang, S., Cao, S.; Shen, S., Pang, Z., Jiang, X. Ligand modified nanoparticles increases cell uptake, alters endocytosis and elevates glioma distribution and internalization. Sci Rep. 2013, 3, 2534,

[151] Kateb B1, Chiu K, Black KL, Yamamoto V, Khalsa B, Ljubimova JY, Ding H, Patil R, Portilla-Arias JA, Modo M, Moore DF, Farahani K, Okun MS, Prakash N, Neman J, Ahdoot D, Grundfest W, Nikzad S, Heiss JD. Nanoplatforms for constructing new approaches to cancer treatment, imaging, and drug delivery: what should be the policy? Neuroimage. 2011 Jan;54 Suppl 1:S106-24.

[152] Danhiera, F., Feronb, O., Préata, V.To exploit the tumor microenvironment: Passive and active tumor targeting of nanocarriers for anti-cancer drug delivery. *Journal of Controlled Release.* 2010, 148, 135–146.

[153] Desai, N., Trieu, V.,Yao, Z., Louie, L., Ci, S.,Yang, A., Tao, C., De, T., Beals, B., Dykes, D., Noker, P., Yao, R., Labao, E., Hawkins, M., Soon-Shiong. Increased antitumor activity, intratumor paclitaxel concentrations, and endothelial cell transport of cremophor-free, albumin-bound paclitaxel, ABI-007, compared with cremophor-based paclitaxel. *Clin Cancer Res*. 2006, 12, 1317-1324.

[154] Pirollo, K. F., Chang, E.H. Does a targeting ligand influence nanoparticle tumor localization or uptake? *Trends Biotechnol*. 2008, 26, 552-558.

[155] Werengowska-Ciećwierz, K., Wiśniewski, M., Terzyk, A. P., Furmaniak, S. The Chemistry of Bioconjugation in Nanoparticles-Based Drug Delivery System. *Advances in Condensed Matter Physics.* 2015, Article ID 198175, 27 pages.

[156] Locatelli, E., Gil, L., Israel, L. L., Passoni, L., Naddaka, M., Pucci, A., Reese, T., Gomez-Vallejo, V., Milani, P., Matteoli, M. Biocompatible nanocomposite for PET/MRI hybrid imaging. *Int J Nanomedicine*. 2012, 7, 6021-6033.

[157] Patel, T., Zhou, J., Piepmeier, J. M., Saltzmanb, W. M. Polymeric Nanoparticles for Drug Delivery to the Central Nervous System. *Adv Drug Deliv Rev*. 2012, 64, 701–705.

[158] Gu, W., Jia, Z., Truong, N. P., Prasadam, I., Xiao, Y., Monteiro, J. M. Polymer Nanocarrier System for Endosome Escape and Timed Release of siRNA with Complete Gene Silencing and Cell Death in Cancer Cells. *Biomacromolecules*, 2013, 14, 3386–3389.

[159] Marin, E., Briceño, M. I., Caballero-George, C. Critical evaluation of biodegradable polymers used in nanodrugs. *Int J Nanomedicine*. 2013, 8, 3071–3091.

[160] Danhier, F., Ansorena, E., Silva, J. M., Coco, R., Le Breton, A., Preat, V. PLGA-based nanoparticles: an overview of biomedical applications. *J Control Release*. 2012, 161, 505-522.

[161] Knop, K., Hoogenboom, R., Fischer, D., Schubert, U. S. Poly(ethylene glycol) in Drug Delivery: Pros and Cons as Well as Potential Alternatives. *Angew Chem Int Ed Engl*. 2010, 49, 6288-6308.

[162] Kunwar, S., Chang, S., Westphal, M.; Vogelbaum, M., Sampson, J., Barnett, G., Shaffrey, M., Ram, Z.; Piepmeier, J., Prados, M. Phase III randomized trial of CED of IL13-PE38QQR vs Gliadel wafers for recurrent glioblastoma. *Neuro Oncol*. 2010, 12, 871-881.

[163] Sawyer, A. J., Saucier-Sawyer, J. K., Booth, C. J., Liu, J., Patel, T., Piepmeier, J. M., Saltzman, W. M. Convection-enhanced delivery of camptothecin-loaded polymer nanoparticles for treatment of intracranial tumors. *Drug Deliv Transl Res*. 2011, 1, 34-42.

[164] Thorne, R. G., Nicholson, C. In vivo diffusion analysis with quantum dots and dextrans predicts the width of brain extracellular space. *Proc Natl Acad Sci U.S.A*. 2006, 103, 5567-5572.

[165] Lippens, G., Najib, J., Wodak, S.J., Tartar, A. NMR sequential assignments and solution structure of chlorotoxin, a small scorpion toxin that blocks chloride channels. *Biochemistry*. 1995, 34,13-21.

[166] Soroceanu, L., Gillespie, Y., Khazaeli, M. B., Sontheimer, H. Use of chlorotoxin for targeting of primary brain tumors. *Cancer Res*. 1998, 58, 4871-4879.

[167] DeBin, J. A., Maggio, J. E., Strichartz, G. R. Purification and characterization of chlorotoxin, a chloride channel ligand from the venom of the scorpion. *Am J Physiol*. 1993, 264, C361-369.

[168] Lui, V. C., Lung, S. S., Pu, J. K., Hung, K. N., Leung, G. K. Invasion of human glioma cells is regulated by multiple chloride channels including ClC-3. *Anticancer Res*. 2010, 30, 4515-4524.

[169] McFerrin, M. B., Sontheimer, H. A role for ion channels in glioma cell invasion. *Neuron Glia Biol*. 2006, 2, 39-49.

[170] Locatelli, E., Broggi, F., Ponti, J., Marmorato, P.; Franchini, F., Lena, S., Franchini, M. C. Lipophilic silver nanoparticles and their polymeric entrapment into targeted-PEG-based micelles for the treatment of glioblastoma. *Adv Healthc Mater*. 2012, 1, 342-347.

[171] Gentili, D., Ori, G. & Franchini, MC. Double phase transfer of gold nanorods for surface functionalization and entrapment into PEG-based nanocarriers. *Chem Commun (Camb)*. 2009, 39, 5874-5876.

[172] Locatelli, E., Naddaka, M., Uboldi, C., Loudos, G., Fragogeorgi, E.; Molinari, V.; Pucci, A.; Tsotakos, T., Psimadas, D.; Ponti, J.; et al. Targeted delivery of silver nanoparticles and alisertib: in vitro and in vivo synergistic effect against glioblastoma. *Nanomedicine (Lond).* 2014, 9, 839-849.

[173] Goldstein, J. L., Anderson, R. G. W., Brown, M. S. Coated pits, coated vesicles, and receptor-mediated endocytosis. *Nature*. 1979, 279, 679 – 685.

[174] Miconi, G., Palumbo, P., Raysi Dehcordi, S., La Torre, C., Lombardi, F., Evtoski, Z., Cimini, A. M., Galzio, R., Cifone, M. G.; Cinque, B. Immunophenotypic characterization of human glioblastoma stem cells: correlation with clinical outcome. *J Cell Biochem*. 2015, 116, 864-876.

[175] Jia, W., Lu, R., Martin, T. A., Jiang, W. G. The role of claudin-5 in blood-brain barrier (BBB) and brain metastases (review). *Mol Med Rep*. 2014, 9, 779-785.

[176] Kwak, S. Y., Kim, B. Y., Ahn, H. J., Yoo, J. O.; Kim, J., Bae, I. H., Han, Y. H. et al. Ionizing radiation-inducible miR-30e promotes glioma cell invasion through EGFR stabilization by directly targeting. *CBL-B. febs J*. 2015, 282, 1512–1525.

[177] Park, C. M., Park, M. J., Kwak, H. J., Lee, H. C.; Kim, M. S., Lee, S. H.; Park, I. C., Rhee, C. H., Hong, S. I. Ionizing radiation enhances matrix metalloproteinase-2 secretion

and invasion of glioma cells through Src/epidermal growth factor receptor-mediated p38/Akt and phosphatidylinositol 3-kinase/Akt signaling pathways. *Cancer Res*. 2006, 66, 8511-8519.

[178] Lee, W. H., Warrington, J. P., Sonntag, W. E., Lee, Y. W. Irradiation alters MMP-2/TIMP-2 system and collagen type IV degradation in brain. *Int J Radiat Oncol Biol Phys*. 2012, 82, 1559-1566.

[179] Bjorklund, M., Koivunen, E. Gelatinase-mediated migration and invasion of cancer cells. *Biochim Biophys Acta*. 2005, 1755, 37-69.

[180] Urbanska, K. , Pajak, B., Orzechowski, A., .Sokolowska, J., Grodzik, M., Sawosz, E., Szmidt, M., Sysa, P. The effect of silver nanoparticles (AgNPs) on proliferation and apoptosis of in ovo cultured glioblastoma multiforme (GBM) cells. *Nanoscale Res Lett*. 2015, 10, 98.

[181] Egusquiaguirre, S. P., Igartua, M., Hernández, R. M., Pedraz, J. L., Nanoparticle delivery systems for cancer therapy: advances in clinical and preclinical research. *Clin Transl Oncol.* 2012, 14, 83-93.

[182] Suka, J. S., Xua, Q., Kima, N., Hanesa, J., Ensigna, L. M. PEGylation as a strategy for improving nanoparticle-based drug and gene delivery. *Advanced Drug Delivery Reviews.* 2015.

[183] Acharya, S., Sahoo, S. K. PLGA nanoparticles containing various anticancer agents and tumour delivery by EPR effect. *Adv Drug Deliv Rev*. 2011, 63, 170-183.

[184] He, J., Liu, Y., Lubman, M. D. Targeting Glioblastoma Stem Cells: Cell Surface Markers. *Curr Med Chem.* 2012, 19, 6050 – 6055.

[185] Shen, H., Ackerman, A. L., Cody, V., Giodini, A., Hinson, E. R., Cresswell, P., Edelson, R. L., Saltzman, W. M., Hanlon, D. J. Enhanced and prolonged cross-presentation following endosomal escape of exogenous antigens encapsulated in biodegradable nanoparticles. Immunology. *Immunology.* 2006, 117, 78-88.

[186] Panyam, J., Zhou, W. Z., Prabha, S., Sahoo, S. K., Labhasetwar, V. Rapid endo-lysosomal escape of poly(DL-lactide-co-glycolide) nanoparticles: implications for drug and gene delivery. *FASEB J*. 2002,16, 1217-1226.

[187] Varkouhia, A. K., Scholteb, M., Storma, G., Haismab, H. J. Endosomal escape pathways for delivery of biologicals. *Journal of Controlled Release.* 2011, 151, 220-228.

[188] Benjaminsen, R. V., Mattebjerg, A. M., Henriksen, J. R., Moghimi, S. M., Andresen, T. L. The Possible “Proton Sponge ” Effect of Polyethylenimine (PEI) Does Not Include Change in Lysosomal pH. *Molecular Therapy*. 2013, 21, 149–157.

[189] Yuan, H., Gaber, M. W., McColgan, T., Naimark, M. D., Kiani, M. F., Merchant, T. E. Radiation-induced permeability and leukocyte adhesion in the rat blood-brain barrier: modulation with anti-ICAM-1 antibodies. *Brain Res*. 2003, 969, 59-69.

[190] d'Avella, D., Cicciarello, R., Albiero, F., Mesiti, M., Gagliardi, M. E., Russi, E., d'Aquino, A., Tomasello, F., d'Aquino, S. Quantitative study of blood-brain barrier permeability changes after experimental whole-brain radiation. *Neurosurgery*. 1992, 30, 30-34.

[191] Hardee, M. E., Zagzag, D. Mechanisms of glioma-associated neovascularization. *Am J Pathol*. 2012, 181, 1126-1141.

[192] Engelhardt, S., Patkar, S., Ogunshola, O. O. Cell-specific blood-brain barrier regulation in health and disease: a focus on hypoxia. *Br J Pharmacol*. 2014, 171, 1210-1230.

[193] Jordan, C. T., Guzman, M. L., Noble, M. Cancer stem cells. *N Engl J Med*. 2006, 355, 1253-1261.

[194] Mannino, M., Chalmers, A. J. Radioresistance of glioma stem cells: intrinsic characteristic or property of the 'microenvironment-stem cell unit'? *Mol Oncol*. 2011, 5, 374-386.

[195] McFerrin, M. B.,; Sontheimer, H. A role for ion channels in glioma cell invasion. *Neuron Glia Biol*. 2006, 2, 39-49.